Angewandte Chemie
Eine Zeitschrift der Gesellschaft Deutscher Chemiker

Supporting Information

Blended Conjugated Host and Unconjugated Dopant Polymers Towards N-type All-Polymer Conductors and High-ZT Thermoelectrics

*J. Han, Y. Jiang, E. Tiernan, C. Ganley, Y. Song, T. Lee, A. Chiu, P. McGuiggan, N. Adams, P. Clancy, T. P Russell, P. E. Hopkins, S. M. Thon, J. D. Tovar, H. E. Katz**

1. General procedures and experimental details.

Chemical reagents (Including solvent and PMMA) were purchased and used as received. All the synthesis procedures were performed under N_2. DPP-CHO was purchased from Derthon OPV Co LTD.

^1H and ^{13}C NMR spectra were recorded on Bruker Advance (400 MHz) spectrometers. ^1H NMR chemical shifts were referenced to tetramethylsilane TMS (0 ppm). Gel permeation chromatography (GPC) was performed on a PL gel MIXED-B LS 300 x 7.5mm x 3 at 150 ºC using trichlorobenzene (TCB) stabilized with 0.0125% BHT as eluent. The EPR measurements were performed on a Bruker-EMX EPR spectrometer at room temperature. Solutions of doped polymers were prepared by stirring at 120 ℃ for 3 min and then 50 μL solution was injected into EPR tubes. Bruker strong pitch sample was used as standard samples. AFM images were taken in tapping mode using a Dimensional 3100 AFM (Bruker Nano, Santa Barbara, CA). The images were visualized using the Nanoscope software (Bruker). The absorption spectra were acquired on an Agilent Cary 5000 UV-Vis-NIR spectrophotometer. For SEM and EDS measurements, all samples were observed under a Tescan MIRA 3 GMU for all SEM images at 20 keV for working distances between 10 and 30 mm. All EDS data were acquired via an AMATEK EDAX Octane Plus.[1] GIWAXS characterization of the thin films was performed at beamline 7.3.3 of Advanced Light Source, Lawrence Berkeley National Laboratory (LBNL). The X-ray beam energy was 10 keV. The sample to detector distance was ~280 mm calibrated with Ag behenate and the incidence angle was 0.16º normalized by a photodiode. All the GIWAXS signals were recorded in Helium atmosphere using a 2D charge-coupled device (CCD) detector (Pilatus 2M) with a pixel size of 0.172 mm by 0.172 mm using x-rays with a wavelength of λ = 1.24 Å. The films of polymers and doped polymers were prepared by drop-casting the solution on silicon

substrates, then annealed at 120 ºC for 12 h, which was similar with the preparation doped devices.[2]

OFET Film Fabrication and Characterization.

Organic field electric transistors (OFETs) with top-gate/bottom-contact (TGBC) configuration were fabricated using n^{++}-Si/SiO2 (300 nm) substrates with a channel length of 200 μm and a channel width of 8000 μm. The substrates were cleaned using ultrasonication in cleaning agent (Decon, labs, Inc), deionized water, acetone, and isopropanol. The cleaned substrates were dried under vacuum at 60 ºC for 6 h and then transferred into a glovebox. The source and drain electrodes comprising a layer of Au (50 nm) were deposited through a shadow mask onto the silicon substrates by thermal evaporation. Thin films of PDPIN (2 mg/mL in orthodichlorobenzene (*o*-DCB)) and doped polymers were prepared by spin coating the solution on the substrates at 2000 rpm for 60 s and annealed at 120 ºC for 30 min. Then, the solution of PMMA was spin-coated on the polymer films at 2000 rpm for 60 s and annealed at 110 ºC for 30 min, resulting in a dielectric layer about 1050 nm thick. Gate electrodes comprising a layer of Au (50 nm) were then deposited through a shadow mask onto the dielectric layer by thermal evaporation. The OFET devices had a channel length (L) of 200 μm and a channel width (W) of 8000 μm. The evaluations of the OFETs were carried out in the ambient atmosphere on a probe stage using an Agilent B1500A as parameter analyzer. The mobility was calculated in the saturation regime according to the equation: $I_{DS} = (W/2L)\mu C_i(V_G - V_T)^2$, where I_{DS} is the drain current, μ is the mobility, and V_G and V_T are the gate voltage and threshold voltage, respectively. Thermal conductivity measurements on the thin film samples were performed via thermoreflectance (TDTR) method.[3]
thermoreflectance (TDTR)

Thermoelectric devices and properties measurements.

ITO electrodes with a channel length of 2 mm and a channel width of 8 mm patterned glass substrates were cleaned by sonication in cleaning agent, deionized water, acetone, and isopropanol. Polymer PDPIN and PSpF were dissolved in *o*-DCB separately with the concentration of 2 and 10 mg mL^{-1}, respectively. N-DMBI was were dissolved in *o*-DCB with the concentration of 2.5 mg mL^{-1}. The polymers and the dopant mixtures were heated at 100 ºC for 24 h to dissolve. Then the polymer was blended with dopant in the desired weight or molar ratio. The mixed solution was heated at 120 ºC and stirred for 2 min. The final solution was dropped on the glass substrates on which 2D wells are fabricated by laying a pattern of Novec polymer. After natural evaporation of solvent in a glove box over 24 h, square films form. The thickness of fims is 60-100 nm, the mean thickness is about 80 nm. The devices were annealed on a hot plate at 120 ºC for 3 h in nitrogen. All the measurements were performed in ambient. Resistance was measured by using a four-probe method with an Agilent B1500A Semiconductor Parameter Analyzer with a channel length of 1000 μm and a channel width of 140 μm. 3-8 measurements of resistance were performed on each sample surface in different positions. Seebeck coefficient can be calculated by $S=\Delta V/\Delta T$ with a channel length of 2000 μm and a channel width of 8000 μm, where ΔV is the thermal voltage obtained between the two electrodes of the device subjected to a temperature gradient ΔT. 2-4 Devices were measured for Seebeck coefficient measurement. Six ΔT were imposed on the sample, so the slopes of ΔV versus ΔT give values of the Seebeck coefficient. The device measurement method is same with the published works.[4]

Thermal conductivity measurement.

Time domain thermoreflectance (TDTR) was used to measure the thermal conductivity of all polymer films. TDTR, the layout of which shown in Figure S1a, is a non-contact, laser-based, pump-probe measurement technique[3a, 5] which monitors the temporal temperature decay of the surface of a sample, and relates this temperature decay to the thermal conductivity of the material under the surface. The rough surfaces of the polymer films would ruin the specular reflection of the TDTR probe beam (c.f., AFM measurements in Figure 6), and thus a bidirectional sample geometry was used for thermal conductivity measurements.[6] In this geometry, an amorphous SiO_2 substrate was first coated with 80 nm of aluminum via electron-beam evaporation. Polymer solutions were then drop cast onto the aluminum transducer and left in a glove box over night to allow the solvent to evaporate. The aluminum layer serves as the optical transducer for TDTR measurements, and the measurement is conducted by focusing the pump and probe from the TDTR measurements at the Al/glass interface which provides a specular reflection. The aluminum time domain thermoreflectance signal is fits to a bidirectional thermal model derived from the solution to the cylindrically symmetric multialyer heat equation.[7]

Our TDTR system is based around the short pulsed sub-picosecond output of a Ti:Sapphire oscillator (Spectra Physics Tsunami), which emits ~100 fs pulses at an 80 MHz repetition rate, which are then split into separate pump and probe paths. The pump pulses are electro-optically modulated to a frequency of 8.4 MHz. Once the pulse train passes through the electro optic modulator (EOM), it is focused to the sample at the Al/glass interface. The probe pulses are delayed in time relative to the pump using a mechanical delay stage. We focus the pump and probe using a 10x objective lens, resulting in focused $1/e^2$ pump and probe radii of

~19 μm and ~11 μm respectively. The reflected probe beam is sent to a balanced photodetector, which is then directed to a lock-in amplifier which monitors the in-phase and out-of-phase voltages of the probe signals referenced to the pump modulation frequency as a function of pump-probe delay time; we monitor the ratio of this in-phase to out-of-phase voltages as a function of pump-probe delay time as shown in Figure S1b.

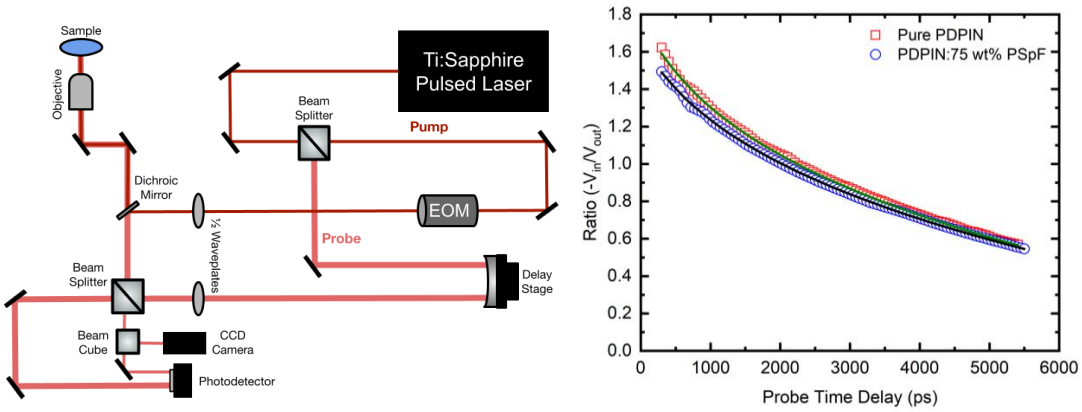

Figure S1: Time Domain Thermoreflectance System and thermal decay curves for the pure PDPIN and 75 wt% PSpF films.

The sensitivity of the measured ratio ($-V_{in}/V_{out}$) to various thermophysical properties of interest was calculated using the logarithmic differentiation method previously published.[8] As shown in Figure S2, we are the most sensitive to the aluminum transducer thickness and the SiO_2 thermal conductivity. These are then followed by the polymer thermal conductivity and heat capacity, which have identical sensitives, since the TDTR signal is sensitive to the thermal effusivity of the polymer. We assume literature heat capacities for the Al transducer and SiO_2 substrate.[9] The Al transducer thickness (d_{Al} = 81 nm) was measured via picosecond ultrasonic[10] and profilometry measurements, and its thermal conductivity (κ_{Al} = 149 W m^{-1}

K^{-1}) was measured using a four-point probe apparatus. The SiO_2 substrate thermal conductivity (κ_{SiO2} = 1.40 W m^{-1} K^{-1}) was experimentally measured using TDTR on a control sample. Since we are sensitive to both the heat capacity and thermal conductivity of the polymer, we must know one in order to fit for the other. The heat capacity of PDPIN, PSpF, and N-DMBI are unknown, so we assumed the heat capacity of P3HT and accounted for any error with an added 20% uncertainty, similar to the procedure used in our prior work.[11] Additional uncertainty, encompassed in the error bars of the thermal conductivity is addressed with a 5% uncertainty in the Al transducer thickness.

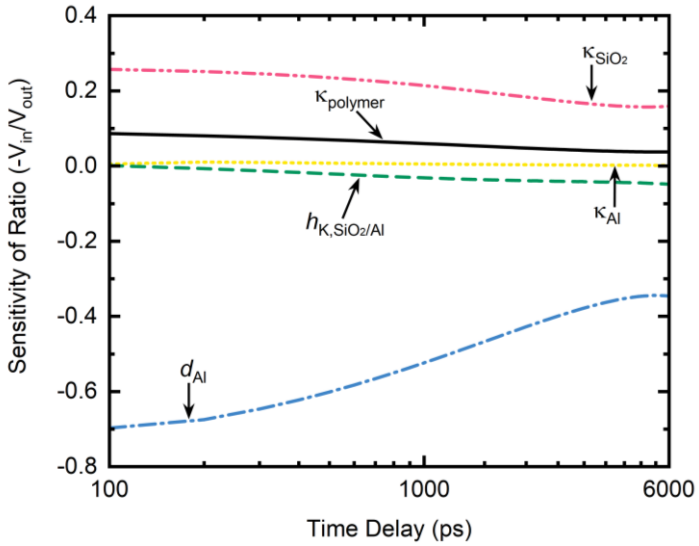

Figure S2: Sensitivity of the ratio of the in-phase (V_{in}) and out-of-phase (V_{out}) signals to specified thermophysical properties of interest, for polymer films at an 8.4 MHz frequency.

We make the assumption in our data analysis that that the thermal conductivities of the polymer films are isotropic, an assumption that has been established in prior works on amorphous and disordered polymers.[12] In our polymer system, there is no preferential orientation nor are there any large crystalline domains, as shown in the GIWAX measurements in Fig. 6a-g, further justifying our assumption of isotropy.

Computational studies.

The ORCA software package (CITE: F. Neese, WIREs Computational Molecular Science 2012, 2, 73-78.) was used to simulate representative structures of the species investigated in this work. Due to the computational rigor required for many-atom simulations at an acceptable level of theory, PDPIN was reduced to its repeat unit, DPIN, TBAF was approximated as TMAF, and PSpF was modeled as MPSpF. To probe the propensity of these species for adduct formation, a raster grid technique similar to previously published works was used[13]. A 4x4 grid of, *e.g.* TMAF, was placed 3 nm above a DPIN molecule in 16 separate simulation environments. ORCA geometry optimization was performed with a B97-D3 functional, a def2-TZVP basis set, and a uniform dielectric of 9.840 applied across the simulation medium to mimic the solvent effects of orthodichlorobenzene. The binding enthalpy was calculated by subtracting the sum of the energies of the geometry-optimized constituent species from the geometry-optimized energy of the complex. In other words, a negative binding enthalpy indicates favorable complexation, *i.e.* that the complex has a lower energy (and is therefore more stable) than its constituent species. Much in the same way, electron affinities and ionization potentials were calculated via a subtractive method. A single-point calculation of a geometry-optimized structure, less or more a single electron, yielded the ionization potential or electron affinity, respectively, after subtracting from the energy of the uncharged structure. Finally, the HOMO and LUMO maps were generated using ORCA DFT output files and the IboView program[14] (find in: http://iboview.org/index.html).

Statistics

1. All the data in this work were processed by the software of OriginLab and without any normalization, except for the absorption spectra.

2. Data presentation: the data error bars were calculated and are shown as standard errors.

3. All the data were measured in different positions and repeated at different times with

different devices. As noted above, for conductivity, at least 2 samples and 3-8 measurements at different positions on every sample; for Seebeck coefficient, at least 2 samples and 2-5 measurements at different positions on every sample.

2. Synthesis of polymer PDPIN.

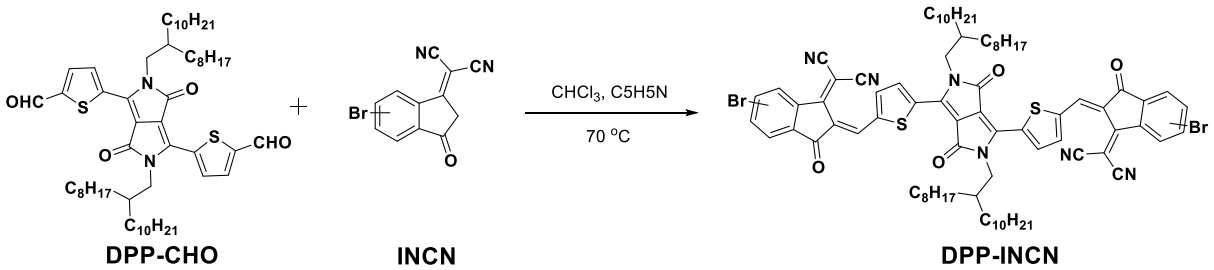

DPP-INCN:

DPP-CHO (0.5 g, 0.545 mmol), INCN (0.5 g, 1.73 mmol), 60 mL chloroform and 4 mL pyridine was added to a dry 200 mL Schlenk bottle, then evacuation and refilling with N_2 was repeated 5 times under stirring. Then the solution was heated to 70 ℃ and reflux for 36 h under dark. When the reaction ended, the organic solution was concentrated with a rotary evaporator and washed with acetone. After dried in vacuum oven at 80 ℃, dark green solid was obtained and in 50% yield. ^{1}H NMR ($C_2D_2Cl_4$, 400 MHz, 100 ℃): δ/ppm: 9.01 (dd, 2H), 8.78 (d, 3H), 8.48 (d, 1H), 7.99 (s, 1H), 7.89 (d, 2H), 7.83 (dd, 2H), 7.72 (d, 1H), 4.11 (d, 4H), 1.94 (s, 2H), 1.14-1.32 (m, 64H), 0.74-0.79 (m, 12H). ^{13}C NMR ($C_2D_2Cl_4$, 100 MHz, 100 ℃)): δ/ppm: 214.63, 189.77, 187.50, 187.26, 162.72, 159.91, 142.83, 137.61, 137.38, 131.70, 127.88, 124.89, 115.08, 114.96, 114.90, 114.44, 48.75, 39.91, 33.13, 30.54, 15.21.

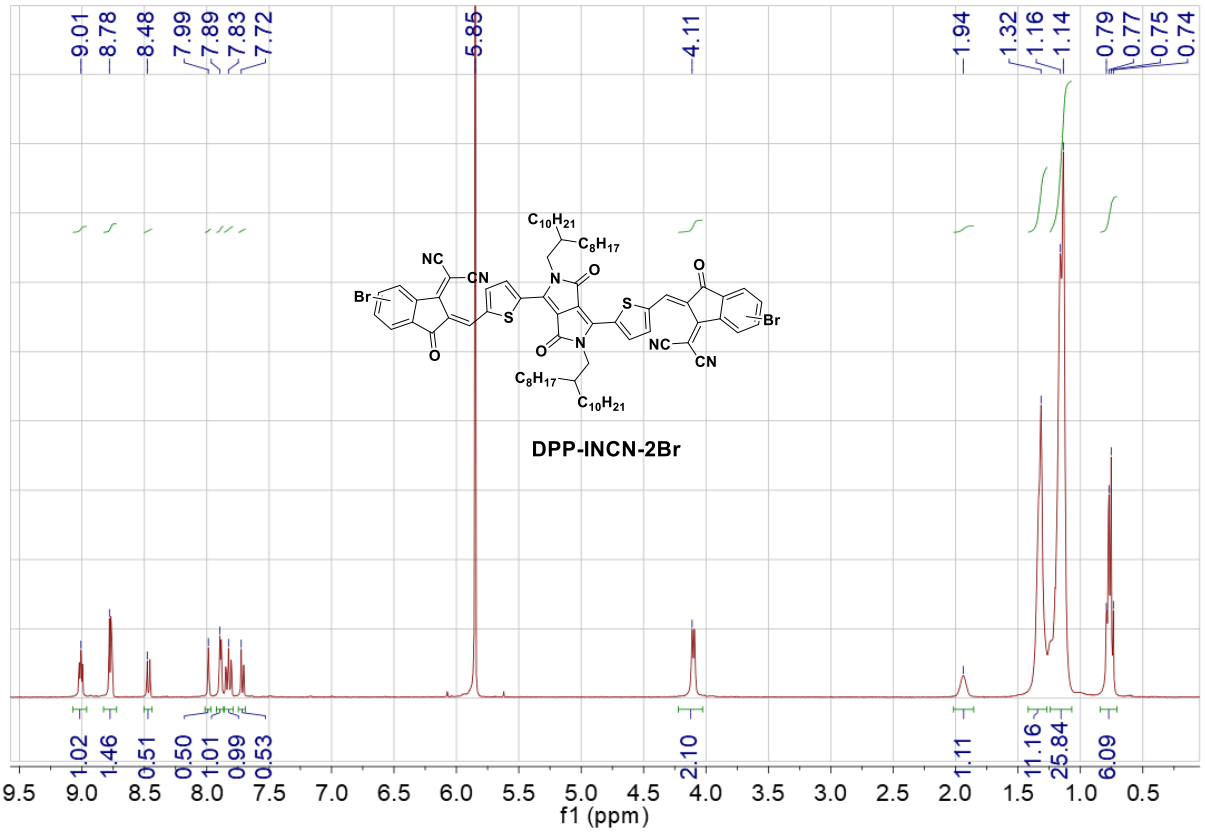
9.01
8.78
8.48
7.99
7.89
7.83
7.72
5.85
4.11
1.94
1.32
1.16
1.14
0.79
0.77
0.75
0.74
1.02
1.46
0.51
0.50
1.01
0.99
0.53
2.10
1.11
11.16
25.84
6.09
DPP-INCN-2Br
f1 (ppm)

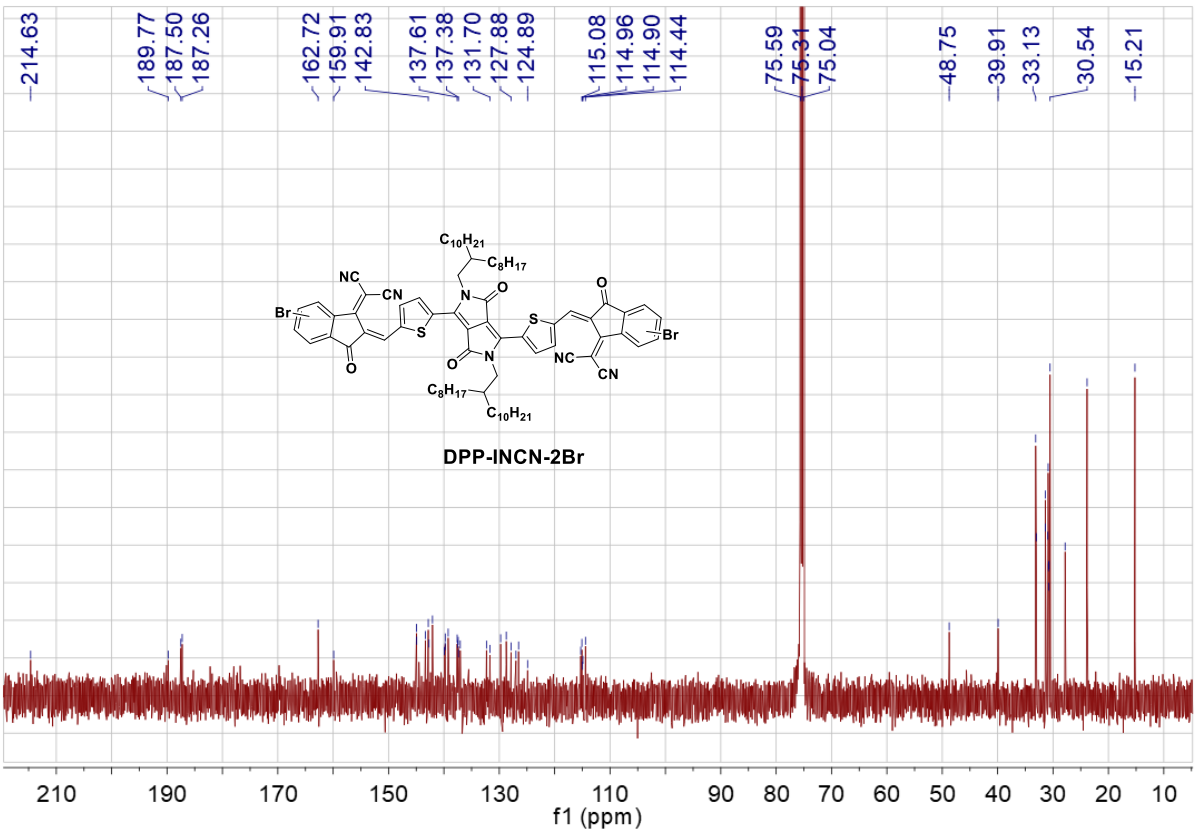
214.63
189.77
187.50
187.26
162.72
159.91
142.83
137.61
137.38
131.70
127.88
124.89
115.08
114.96
114.90
114.44
75.59
75.31
75.04
48.75
39.91
33.13
30.54
15.21
DPP-INCN-2Br
f1 (ppm)

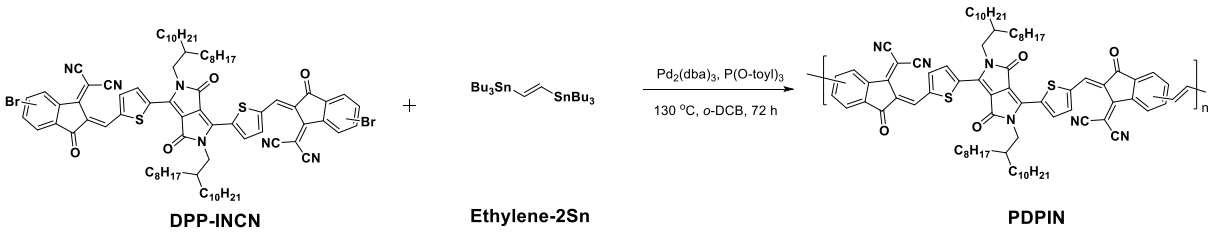

PDPIN:

DPP-INCN (160 mg, 0.112 mmol) and Ethylene-2Sn (72 mg, purity: 90-95%) was added to a dried 10 mL Schlenk tube under N_2. Then $Pd_2(dba)_3$ (5.6 mg), $P(o\text{-}tol)_3$ (8.4 mg) and 8 mL *o*-DCB was added in the N_2 glove box. Then the tube was evacuated and refilled with N_2 for 3 times. The reaction mixture was stirred for 72 h at 130 ℃, then 0.2 mL bromobenzene was added and reacted for another 12 h. The polymer was washed in a Soxhlet extractor with methanol, acetone and hexane for 24 h, respectively. The final product was dried in vacuum at 70 ℃ to achieve a black solid in yield of 84.9%. GPC: M_w = 122 kDa, M_n = 28 kDa, *PDI* = 4.4. The NMR integral ratios of total aliphatic to aryl/vinyl peaks are close to the expected value of 5:1.

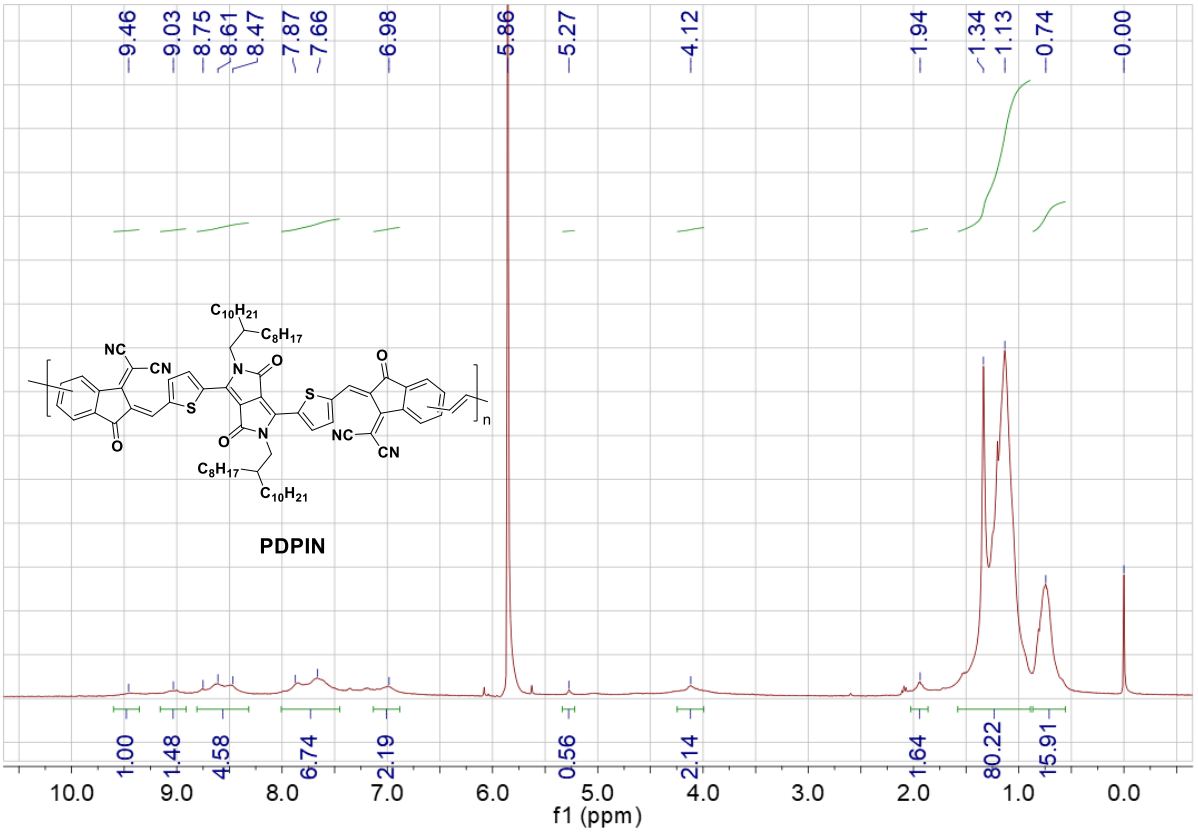

3. Characteristics of polymer PDPIN and doped polymer films.

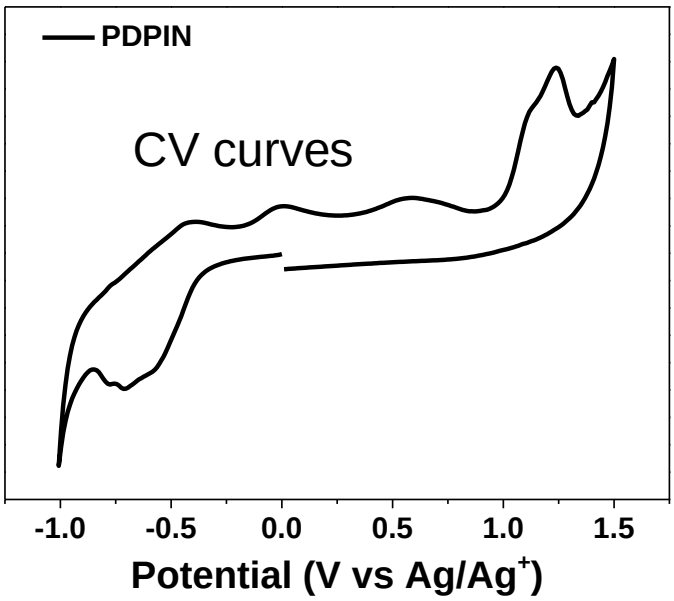

Figure S3. CV curves of PDPIN. The peak at 0.5 V is presumably an aggregate or impurity oxidation. The energy levels of PDPIN were calculated according to the equations $E_{HOMO} = -e(E_{ox} + 4.60)$ and $E_{LUMO} = -e(E_{red} + 4.60)$.

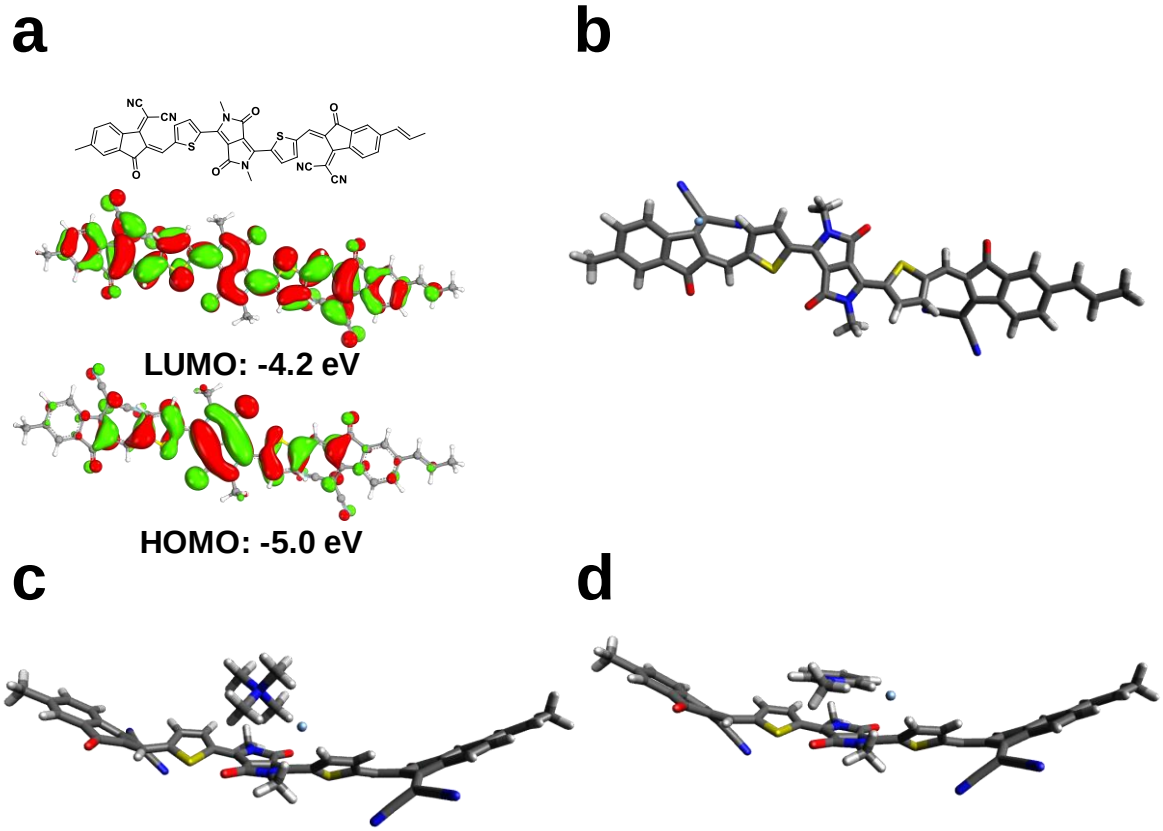

Figure S4. a)The frontier molecular orbital wave function distribution and energy levels of repeat unit of PDPIN. The images of geometry optimizations with the most favorable binding energy for adducts of b) DPIN-F, c) DPIN-TMAF, and d) DPIN-MPSpF.

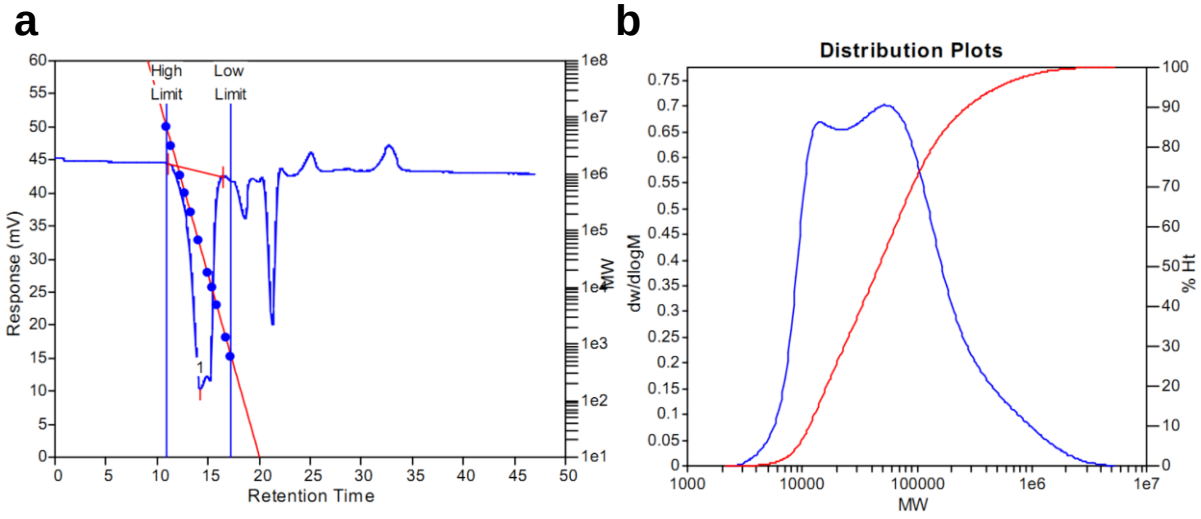

Figure S5. GPC traces of PDPIN at 150 ℃ with TCB as eluent, with polystyrene standards.

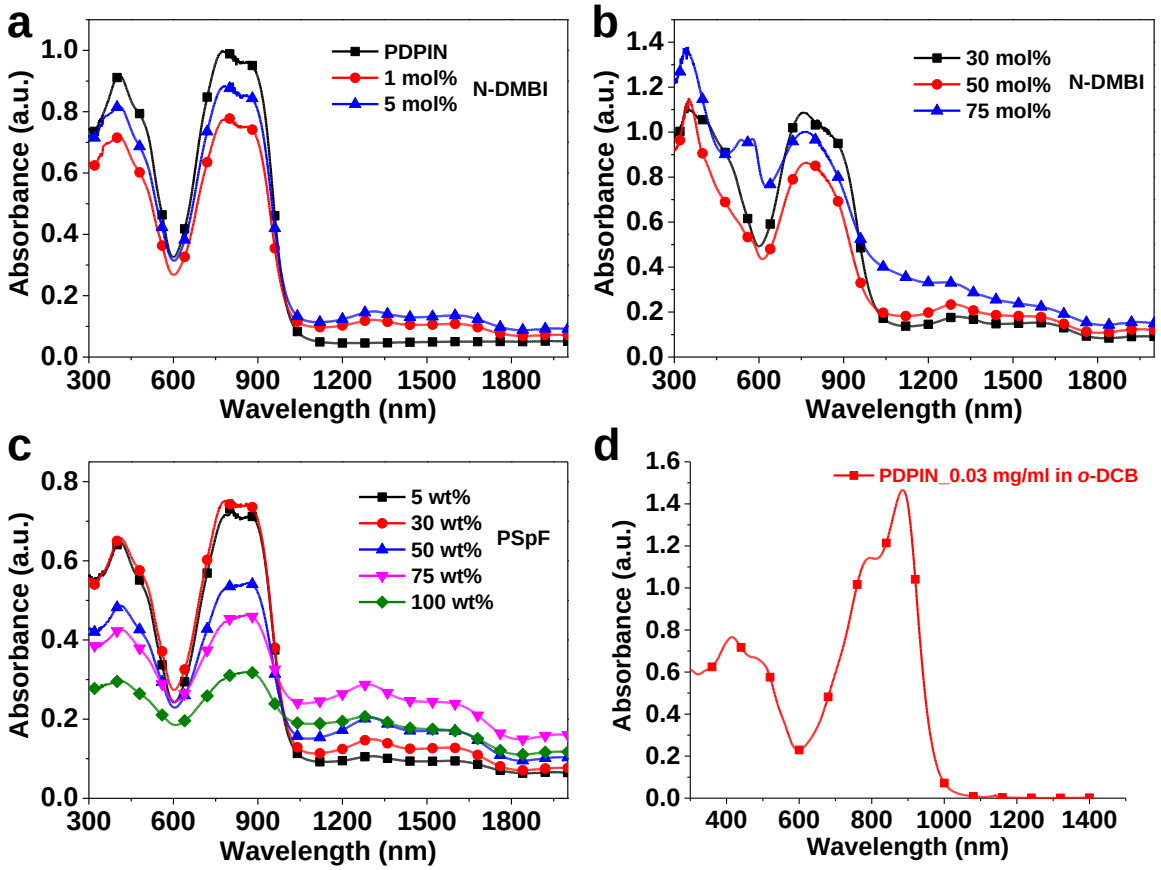

Figure S6. a) and b) The absorption spectra of pristine PDPIN and N-DMBI doped PDPIN with different N-DMBI/PDPIN molar ratos in films. c) The absorption spectra of PSpF doped PDPIN with different PSpF/PDPIN weight ratios. d) The absorption spectra of PDPIN in *o*-DCB with a concentration of 0.03 mg/mL. The weight ratio in this work means the weight of polymer dopant PSpF/the weight of conjugated polymer PDPIN, for example, the 100 wt% PSpF sample means the weight ratio of dopant and host is 1/1.

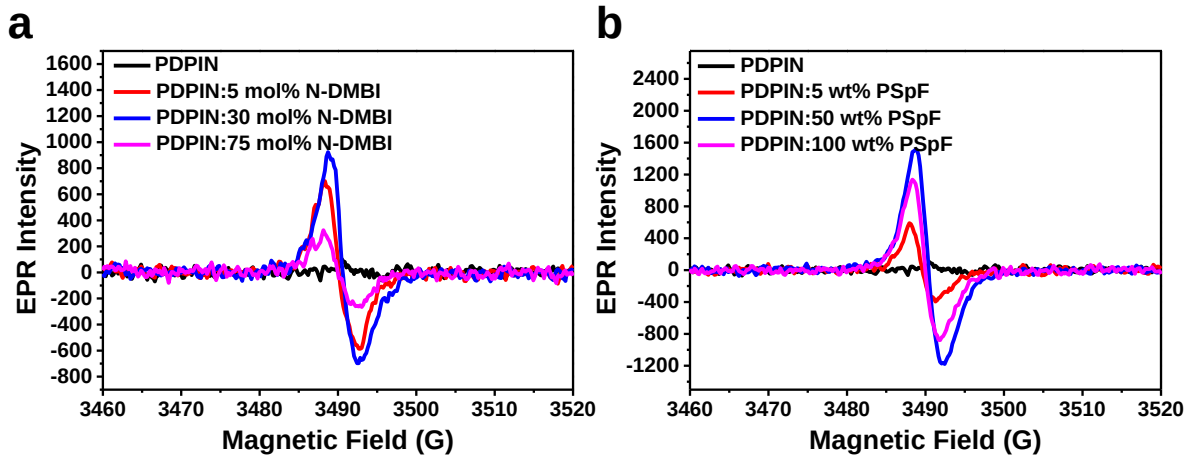

Figure S7. a) The EPR spectra of pristine and N-DMBI doped PDPIN with different molar ratios. b) The EPR spectra of pristine and PSpF doped PDPIN with different weight ratios.

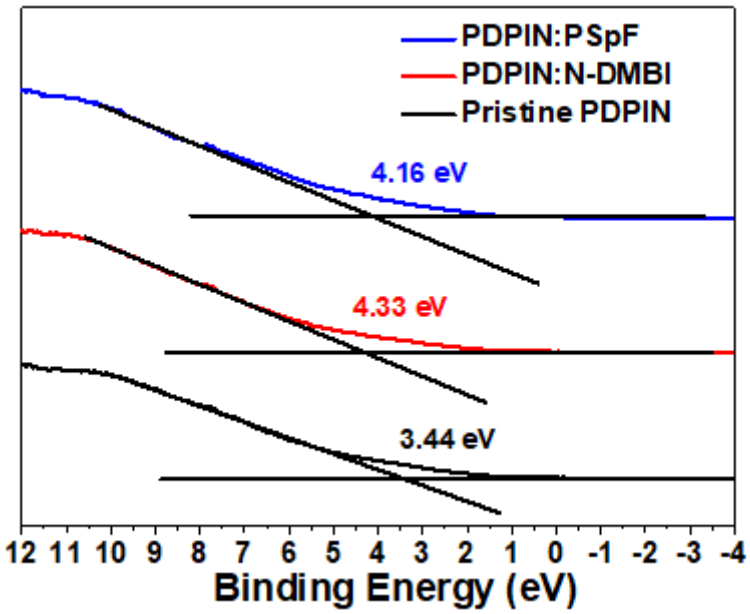

Figure S8. The low-binding energy region (valence band) of UPS spectra.

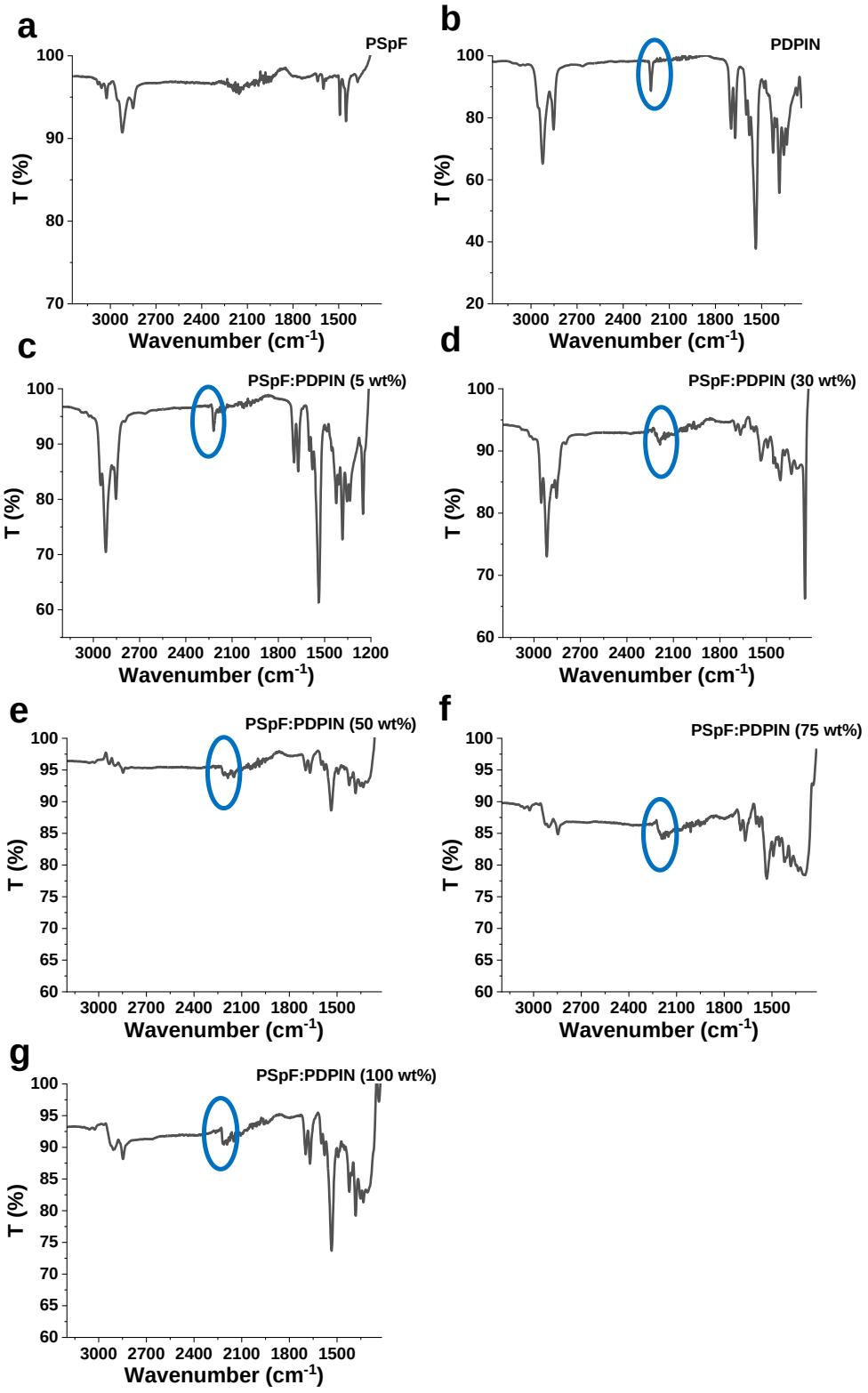

Figure S9. The IR spectra of a) PSpF, b) PDPIN, and c) 5, d) 30, e) 50, f) 75 and g) 100 wt% PSpF-doped PDIN films.

Table S1. The DFT calculation results of adduct of DPIN-F.

Filename	Adduct Binding Energy Geom Opt Energy (Ha)	Δ (eV)	Ionization Energy IE Energy (Ha)	Δ (eV)	Electron Affinity EA Energy (Ha)	Δ (eV)
DPIN_oDCB_sp_F_ion_01	-3293.7	0.0	-3293.5	5.0	-3293.8	-3.8
DPIN_oDCB_sp_F_ion_02	-3293.7	-0.6	-3293.5	4.9	-3293.8	-3.6
DPIN_oDCB_sp_F_ion_03	-3293.7	-0.6	-3293.5	4.9	-3293.8	-3.6
DPIN_oDCB_sp_F_ion_04	-3293.7	0.0	-3293.5	5.0	-3293.8	-3.8
DPIN_oDCB_sp_F_ion_05	-3293.7	0.0	-3293.5	5.0	-3293.8	-3.8
DPIN_oDCB_sp_F_ion_06	-3293.7	-0.4	-3293.5	5.0	-3293.8	-3.7
DPIN_oDCB_sp_F_ion_07	-3293.7	-0.4	-3293.5	5.0	-3293.8	-3.7
DPIN_oDCB_sp_F_ion_08	-3293.7	-0.4	-3293.5	5.0	-3293.8	-3.7
DPIN_oDCB_sp_F_ion_09	-3293.7	-0.4	-3293.5	5.0	-3293.8	-3.7
DPIN_oDCB_sp_F_ion_10	-3293.7	0.0	-3293.5	5.0	-3293.8	-3.8
DPIN_oDCB_sp_F_ion_11	-3293.7	-0.4	-3293.5	5.0	-3293.8	-3.7
DPIN_oDCB_sp_F_ion_12	-3293.7	0.0	-3293.5	5.0	-3293.8	-3.8
DPIN_oDCB_sp_F_ion_13	-3293.7	0.0	-3293.5	5.0	-3293.8	-3.8
DPIN_oDCB_sp_F_ion_14	-3293.7	-0.3	-3293.5	5.1	-3293.8	-3.8

Table S2. The DFT calculation results of adduct of DPIN-TMAF.

Filename	Adduct Binding Energy Geom Opt Energy (Ha)	Δ (eV)	Ionization Energy IE Energy (Ha)	Δ (eV)	Electron Affinity EA Energy (Ha)	Δ (eV)
DPIN_oDCB_sp_TMAF_oDCB_sp_00	-3507.9	-0.1	-3507.7	5.2	-3508.0	-3.8
DPIN_oDCB_sp_TMAF_oDCB_sp_01	-3507.9	-0.4	-3507.7	5.3	-3508.0	-3.8
DPIN_oDCB_sp_TMAF_oDCB_sp_02	-3507.9	-0.4	-3507.7	5.2	-3508.0	-3.8
DPIN_oDCB_sp_TMAF_oDCB_sp_03	-3507.9	-0.4	-3507.7	5.3	-3508.0	-3.9
DPIN_oDCB_sp_TMAF_oDCB_sp_04	-3507.9	-0.4	-3507.7	5.4	-3508.0	-3.9
DPIN_oDCB_sp_TMAF_oDCB_sp_05	-3507.9	-0.4	-3507.7	5.4	-3508.0	-3.9
DPIN_oDCB_sp_TMAF_oDCB_sp_06	-3507.9	-0.4	-3507.7	5.4	-3508.0	-3.9
DPIN_oDCB_sp_TMAF_oDCB_sp_08	-3507.9	-0.4	-3507.7	5.3	-3508.0	-3.9
DPIN_oDCB_sp_TMAF_oDCB_sp_09	-3507.9	-0.2	-3507.7	5.3	-3508.0	-3.9
DPIN_oDCB_sp_TMAF_oDCB_sp_10	-3507.8	1.5	-3507.6	5.7	-3507.9	-3.3
DPIN_oDCB_sp_TMAF_oDCB_sp_13	-3507.9	-0.2	-3507.7	5.4	-3508.0	-4.0
DPIN_oDCB_sp_TMAF_oDCB_sp_14	-3507.9	-0.2	-3507.7	5.4	-3508.0	-4.0
DPIN_oDCB_sp_TMAF_oDCB_sp_15	-3507.9	-0.2	-3507.7	5.4	-3508.0	-4.0

Table S3. The DFT calculation results of adduct of DPIN-MPSpF.

Filename	Adduct Binding Energy Geom Opt Energy (Ha)	Δ (eV)	Ionization Energy IE Energy (Ha)	Δ (eV)	Electron Affinity EA Energy (Ha)	Δ (eV)
DPIN_oDCB_sp_MPSpF_00	-3581.7	-0.4	-3581.5	5.1	-3581.8	-3.6
DPIN_oDCB_sp_MPSpF_01	-3581.7	-0.3	-3581.5	5.3	-3581.8	-3.9
DPIN_oDCB_sp_MPSpF_02	-3581.7	-0.4	-3581.5	5.3	-3581.8	-3.9
DPIN_oDCB_sp_MPSpF_03	-3581.7	-0.5	-3581.5	5.3	-3581.8	-3.9
DPIN_oDCB_sp_MPSpF_04	-3581.7	-0.6	-3581.5	5.4	-3581.8	-4.0
DPIN_oDCB_sp_MPSpF_05	-3581.7	-0.6	-3581.5	5.4	-3581.8	-3.9
DPIN_oDCB_sp_MPSpF_06	-3581.7	-0.1	-3581.5	4.7	-3581.8	-3.5
DPIN_oDCB_sp_MPSpF_07	-3581.7	-0.5	-3581.5	5.3	-3581.8	-4.0
DPIN_oDCB_sp_MPSpF_08	-3581.7	-0.7	-3581.5	5.4	-3581.8	-3.9
DPIN_oDCB_sp_MPSpF_09	-3581.7	-0.5	-3581.5	5.3	-3581.8	-3.9
DPIN_oDCB_sp_MPSpF_11	-3581.7	-0.2	-3581.5	5.3	-3581.8	-3.9
DPIN_oDCB_sp_MPSpF_12	-3581.7	-0.5	-3581.5	5.4	-3581.8	-4.0
DPIN_oDCB_sp_MPSpF_14	-3581.7	-0.3	-3581.5	5.3	-3581.8	-3.9
DPIN_oDCB_sp_MPSpF_15	-3581.7	-0.4	-3581.5	5.4	-3581.8	-4.0

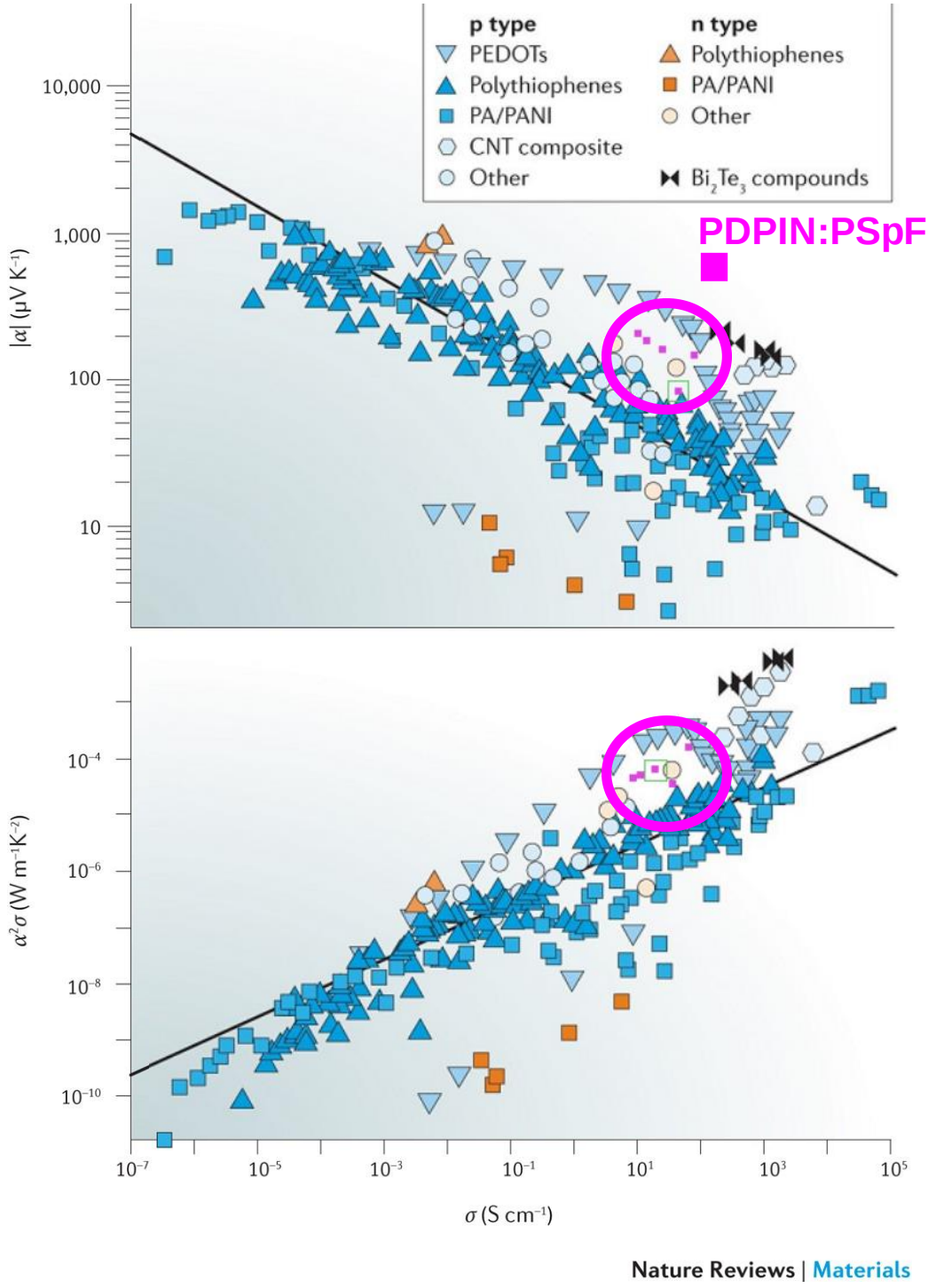

Figure S10. Seebeck coefficient (α; top) and power factor (α2σ; bottom) as functions of conductivity (σ) for a range of doped organic thermoelectric (OTE) polymers and composites summarized by Boris Russ et al.[15] Original figure copyright Springer-Nature.

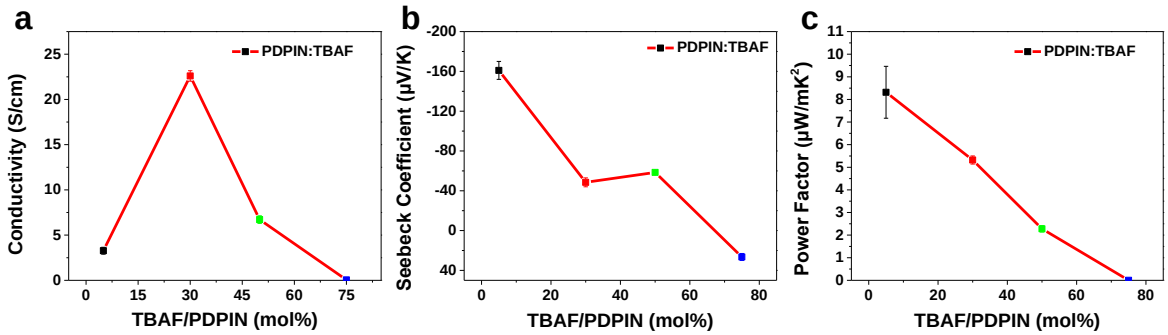

Figure S11. The a) electrical conductivity, b) Seebeck coefficient and c) power factor of TBAF doped PDPIN films.

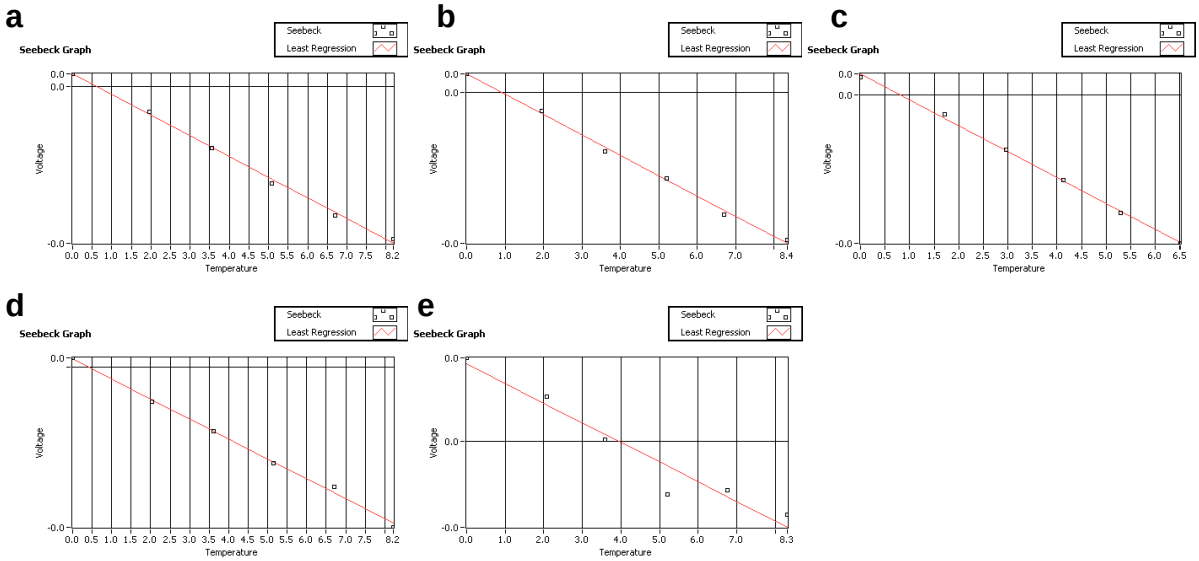

Figure S12. The raw files of Seebeck coefficient plots of a) 1, b) 5, c) 30, d) 50 and e) 75 mol% N-DMBI doped PDPIN.

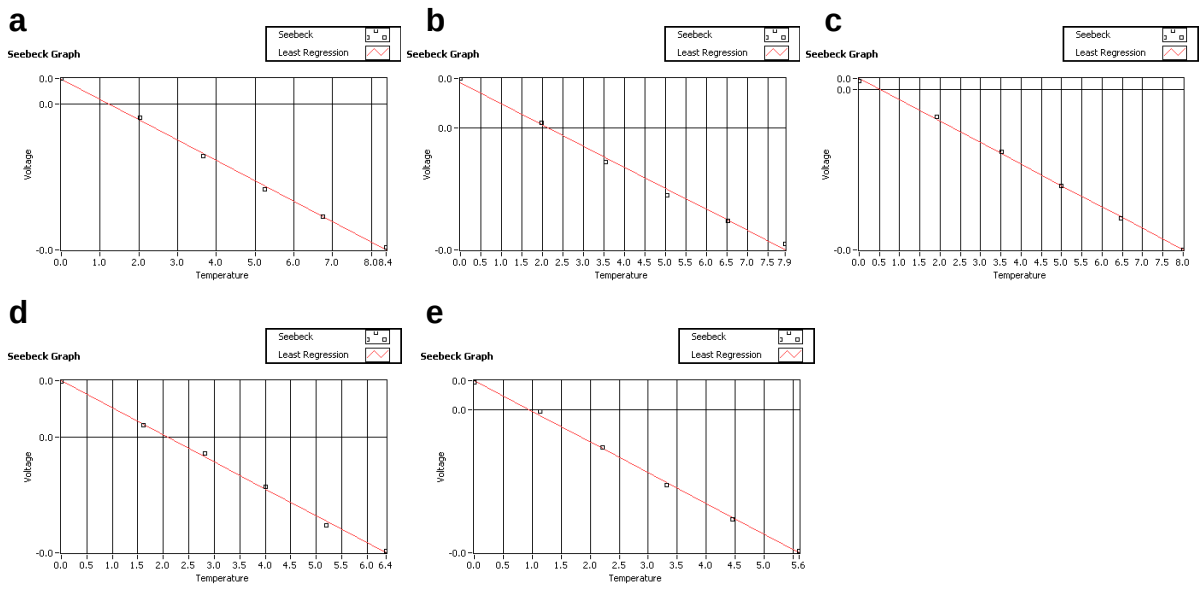

Figure S13. The raw files of Seebeck coefficient plots of a) 5, b) 30, c) 50, d) 75 and e) 100 wt% PSpF doped PDPIN.

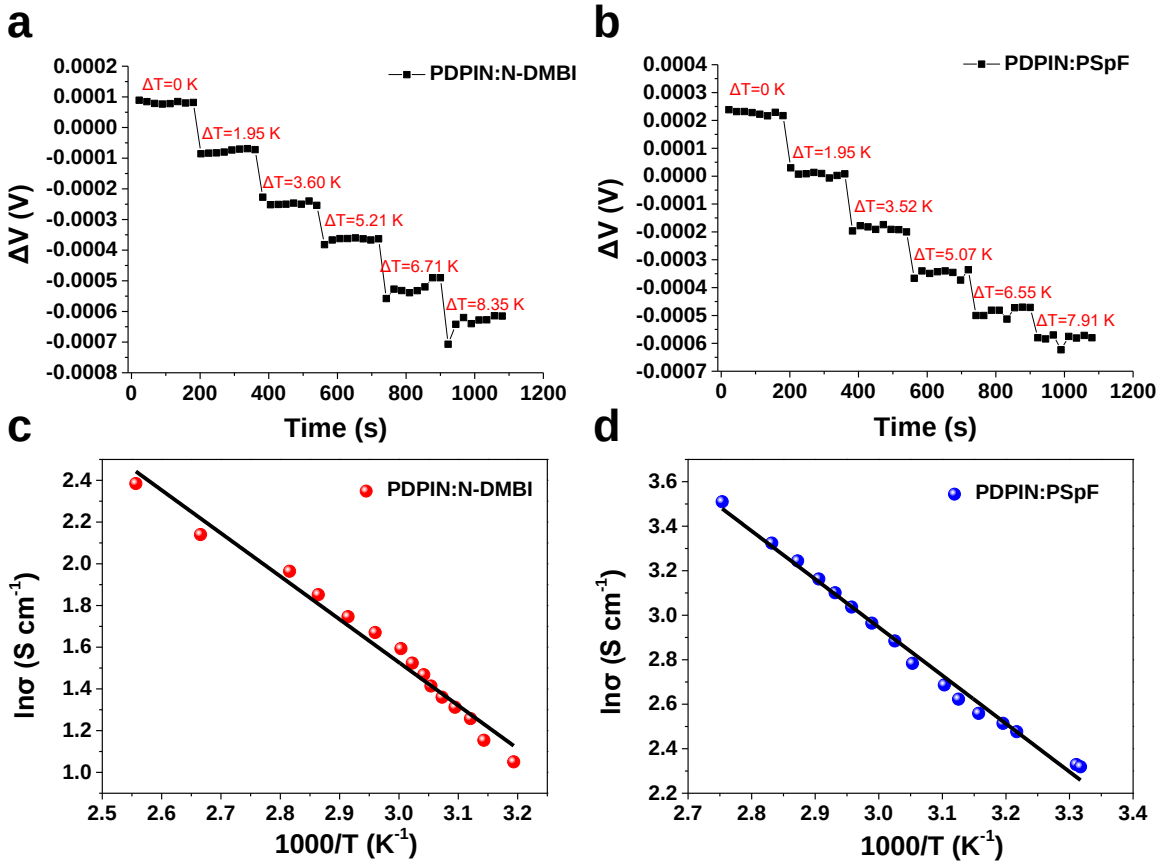

Figure S14. The time-dependent thermal voltage responses of a) N-DMBI and b) PSpF-doped PDPIN. The temperature-dependent σ values of c) 5 mol% N-DMBI and d) 75 wt% PSpF doped PDPIN.

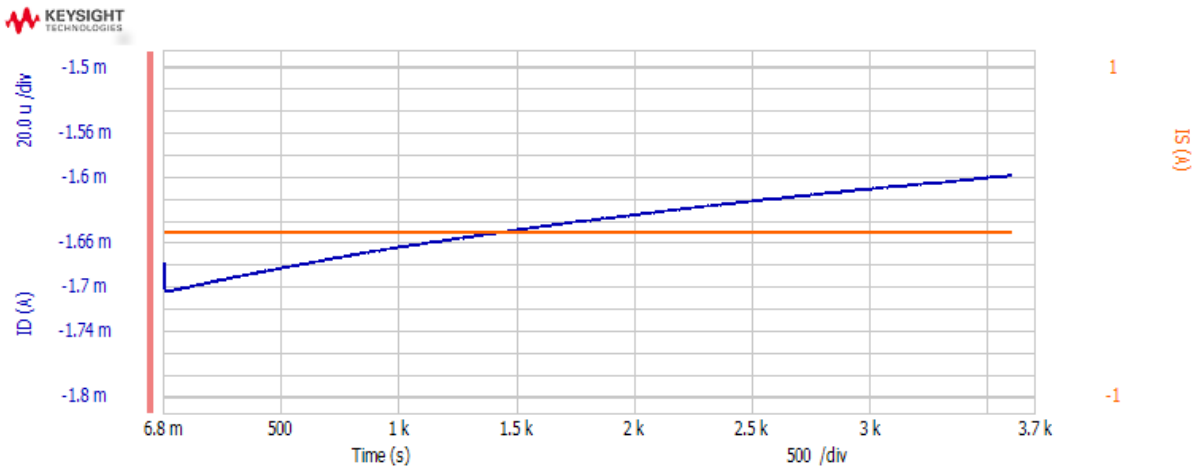

Figure S15. The raw file of time (1 h)-dependent current response of 75 wt% PSpF doped PDPIN under -50 V.

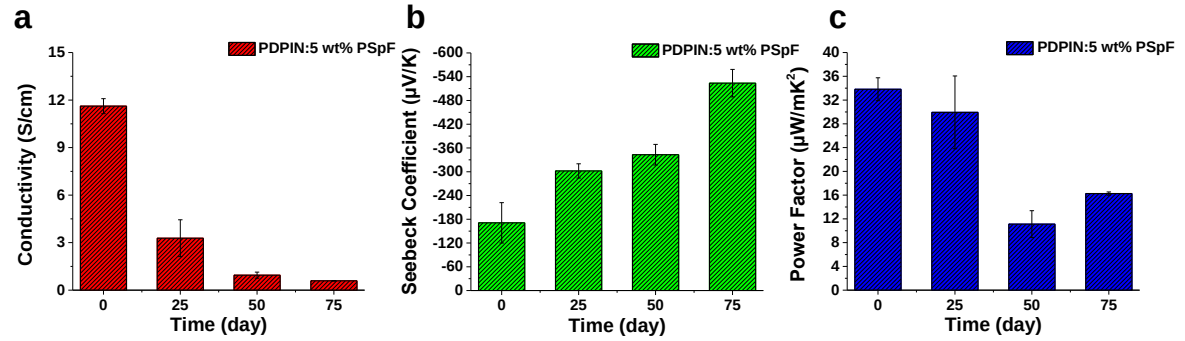

Figure S16. Air stability of a) electrical conductivity, b) Seebeck coefficient and c) Power factor of 5 wt% PSpF doped PDPIN films.

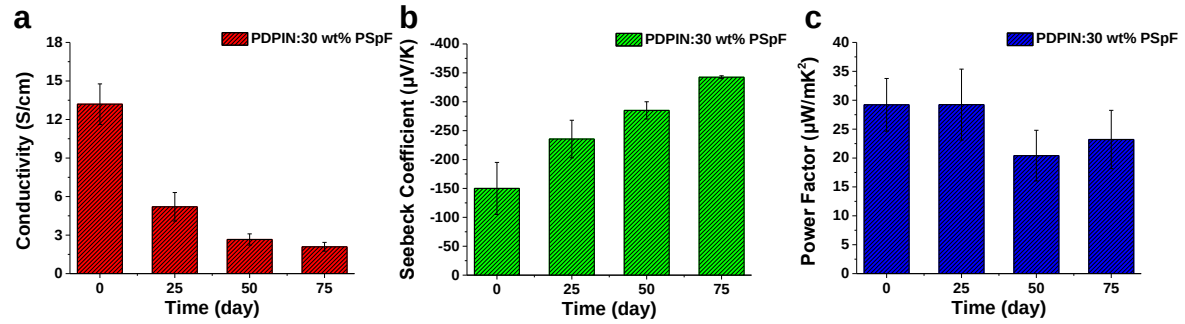

Figure S17. Air stability of a) electrical conductivity, b) Seebeck coefficient and c) Power factor of 30 wt% PSpF doped PDPIN films.

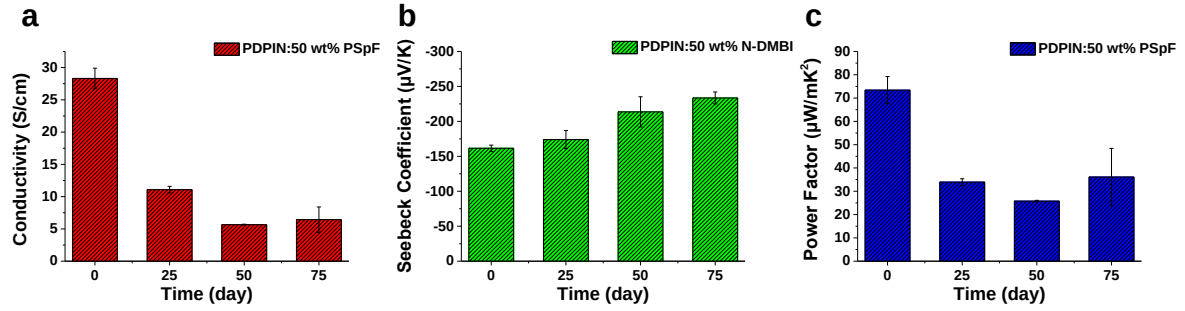

Figure S18. Air stability of a) electrical conductivity, b) Seebeck coefficient and c) Power factor of 50 wt% PSpF doped PDPIN films.

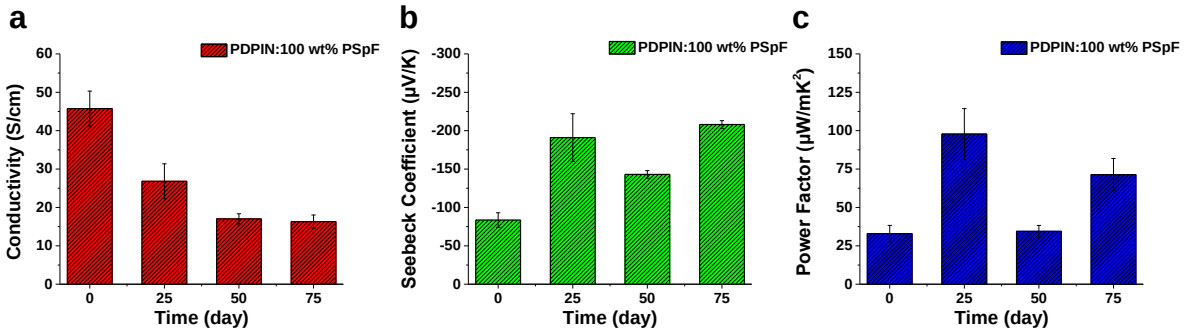

Figure S19. Air stability of a) electrical conductivity, b) Seebeck coefficient and c) Power factor of 100 wt% PSpF doped PDPIN films.

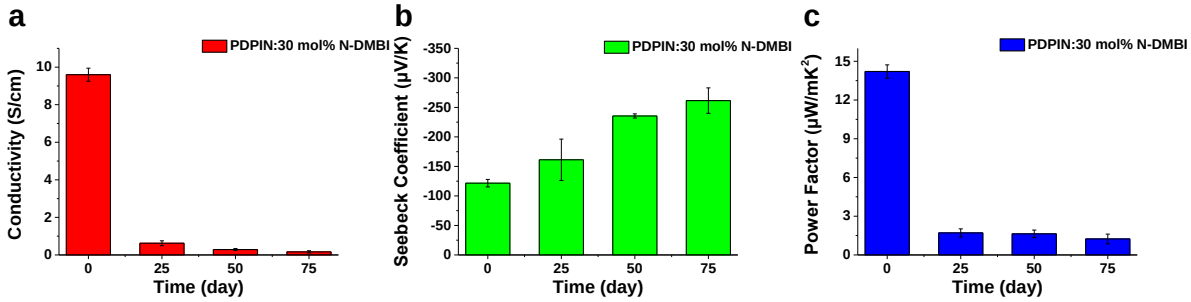

Figure S20. Air stability of a) electrical conductivity, b) Seebeck coefficient and c) Power factor of 30 mol% N-DMBI doped PDPIN films.

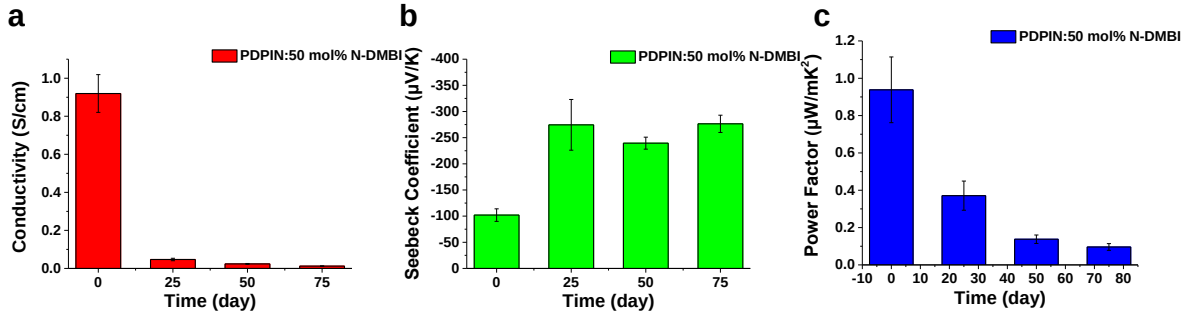

Figure S21. Air stability of a) electrical conductivity, b) Seebeck coefficient and c) Power factor of 50 mol% N-DMBI doped PDPIN films.

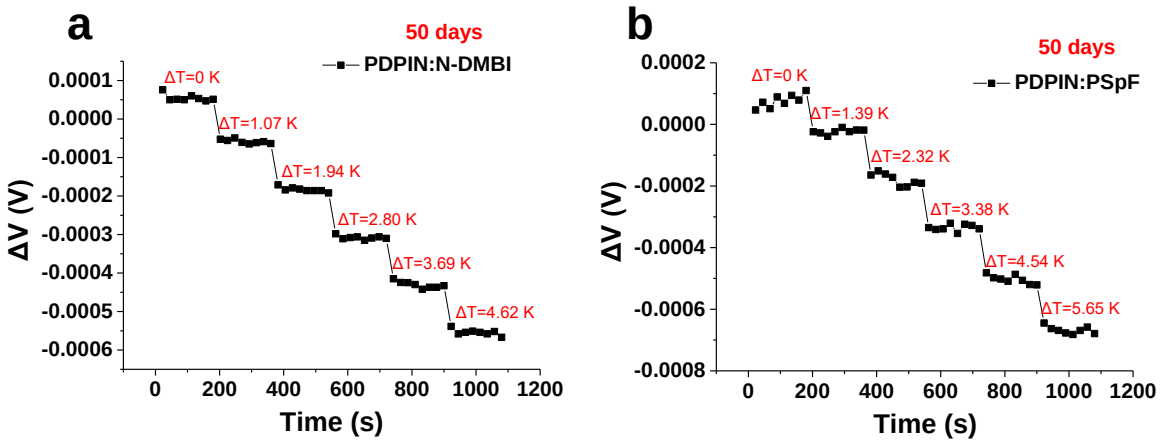

Figure S22. The time-dependent thermal voltage responses of a) N-DMBI and b) PSpF-doped PDPIN after 50 days storing in ambient.

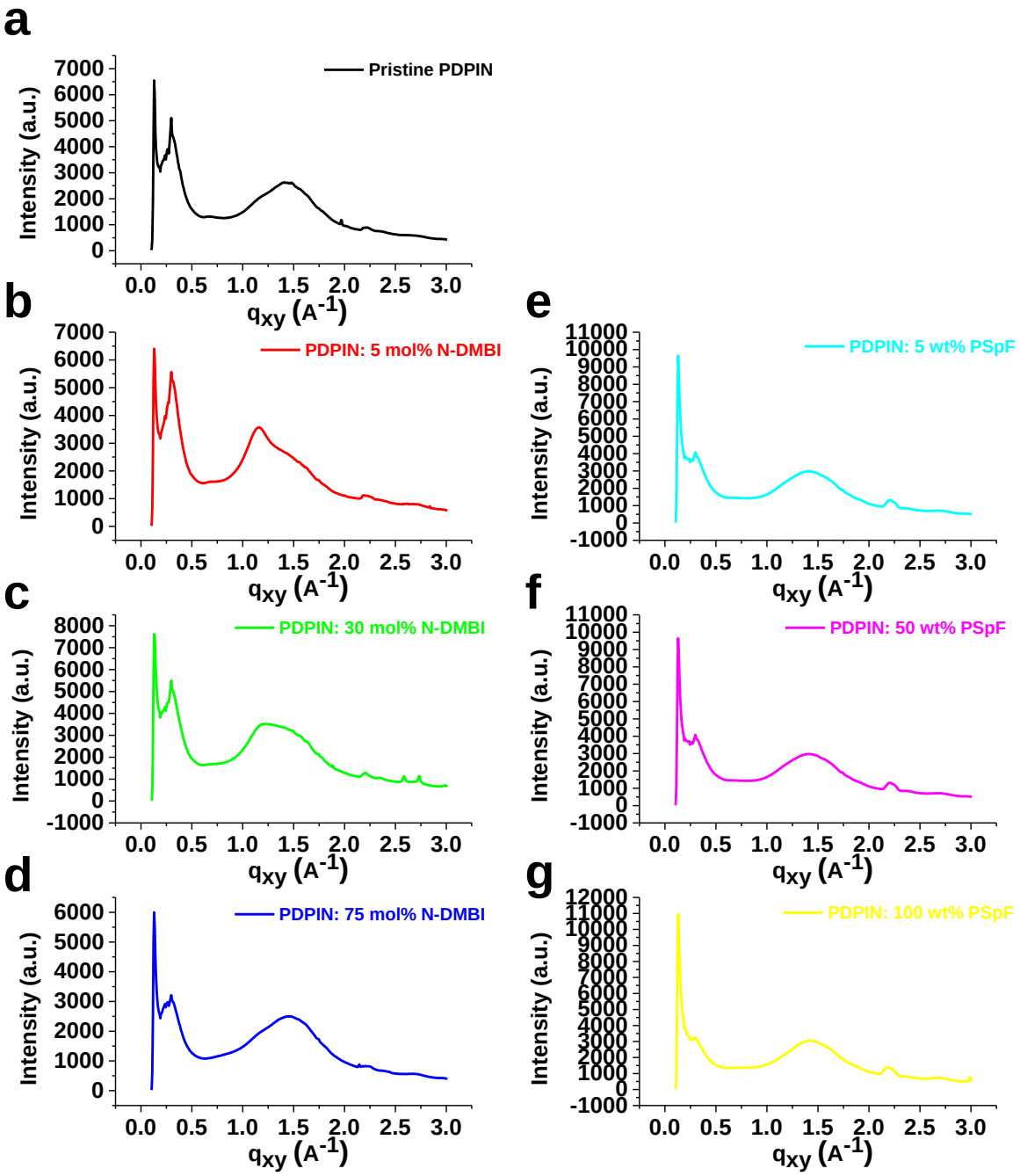

Figure S23. Scattering profiles of in-plane for a) pristine PDPIN, b) 5, c) 30 and d) 75 mol% N-DMBI doped PDPIN films, and e) 5, f) 50 and 100 wt% PSpF doped PDPIN films.

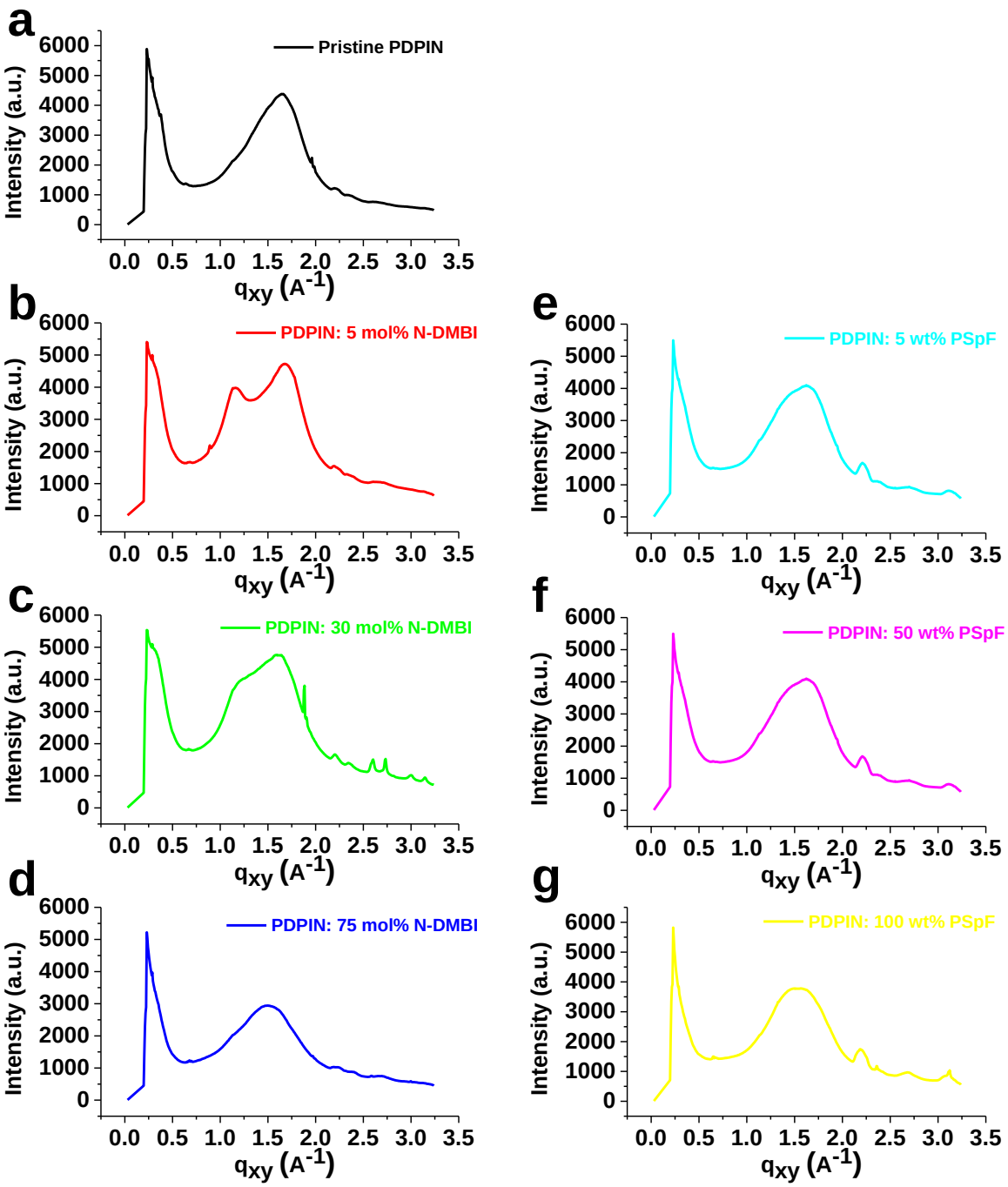

Figure S24. Scattering profiles of out-of-plane for a) pristine PDPIN, b) 5, c) 30 and d) 75 mol% N-DMBI doped PDPIN films, and e) 5, f) 50 and 100 wt% PSpF doped PDPIN films.

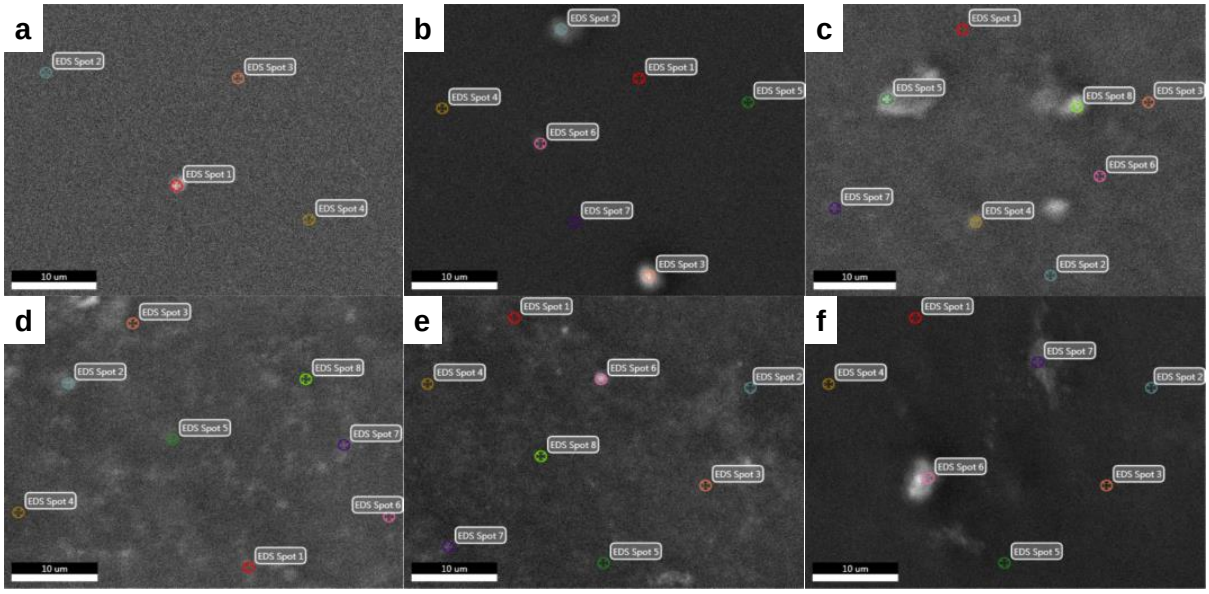

Figure S25. SEM images of a) 5, b) 30, c) 50, d) 75 and e) 100 wt% PSpF doped PDPIN films. The films were prepared with drop-casting method.

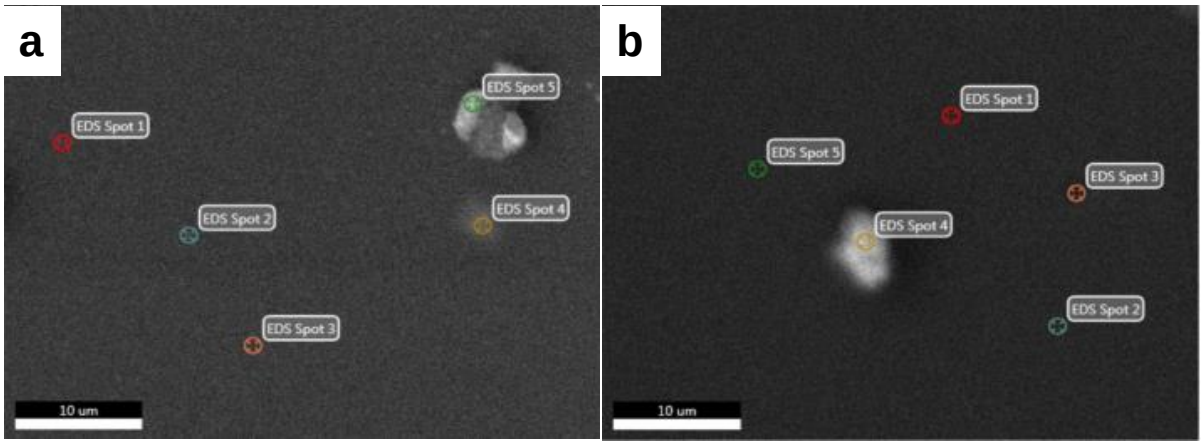

Figure S26. SEM images of a) 5 and b) 50 mol% N-DMBI doped PDPIN films. The films were prepared with drop-casting method.

Table S4. EDS element analysis of pristine PDPIN film in different spots.

	Spot 1	**Spot 2**	**Spot 3**	**Spot 4**
Element	**Atomic %**	**Atomic %**	**Atomic %**	**Atomic %**
C K	25.55	27.81	30.74	29.89
N K	15.96	11.67	10.46	10.92
O K	26.91	17.57	15.08	14.85
Si K	31.08	42.65	43.42	44
S K	0.31	0.12	0.13	0.14
Cr K	0.19	0.18	0.17	0.2

Table S5. EDS element analysis of 5 wt% PSpF doped PDPIN film in different spots.

	Spot 1	Spot 4	Spot 5	Spot 6	Spot 7
Element	**Atomic %**	**Atomic %**	**Atomic %**	**Atomic %**	**Atomic %**
C K	44.13	41.38	43.22	44.96	43.92
N K	7.75	8.37	8.26	9.39	7.76
O K	10.14	10.86	10.1	11.85	10.06
F K	0.01	0.02	0.01	0.18	0.02
Si K	37.69	39.07	38.1	33.23	37.92
S K	0.2	0.19	0.22	0.28	0.22
Cr K	0.08	0.12	0.09	0.11	0.11

Table S6. EDS element analysis of 30 wt% PSpF doped PDPIN film in different spots.

	Spot 2	Spot 3	Spot 4	Spot 5	Spot 7	Spot 8
Element	**Atomic %**	**Atomic %**	**Atomic %**	**Atomic %**	**Atomic %**	**Atomic %**
C K	54.52	50.37	57.45	53.68	51.54	56.63
N K	6.1	6.82	7.87	7.57	7.15	9.01
O K	6.52	8.08	8.79	9.32	8.17	10.85
F K	0.01	0.01	0.17	0.17	0.03	4.8
Si K	32.15	34.06	24.72	27.78	32.43	17.56
S K	0.34	0.26	0.61	0.52	0.29	0.53
Cr K	0.16	0.17	0.14	0.22	0.16	0.16

Table S7. EDS element analysis of 50 wt% PSpF doped PDPIN film in different spots.

	Spot 1	Spot 2	Spot 5	Spot 6	Spot 7	Spot 8
Element	**Atomic %**	**Atomic %**	**Atomic %**	**Atomic %**	**Atomic %**	**Atomic %**
C K	57.84	58.93	58.03	63.82	57.25	62.83
N K	5.79	6.51	6.24	4.79	5.78	4.92
O K	5.6	6.86	6.43	4.68	5.87	4.88
F K	0.02	0.21	0.02	0	0.02	0
Si K	28.98	24.45	27.35	26.18	29.36	26.9
S K	0.68	0.68	0.61	0.36	0.56	0.32
Cr K	0.2	0.18	0.19	0.16	0.2	0.15

Table S8. EDS element analysis of 75 wt% PSpF doped PDPIN film in different spots.

	Spot 1	Spot 2	Spot 3	Spot 6	Spot 7	Spot 8
Element	**Atomic %**	**Atomic %**	**Atomic %**	**Atomic %**	**Atomic %**	**Atomic %**
C K	65.96	63.48	60.11	65.19	67.5	62.97
N K	4.84	4.65	5.76	4.52	4.62	4.47
O K	3.88	3.8	5.78	6.32	4.36	4.07
F K	0.02	0.01	0.02	0.79	0.09	0
Si K	23.6	25.92	26.94	16.62	20.46	27.09
S K	0.66	0.78	0.47	0.88	0.73	0.57
Cr K	0.18	0.17	0.16	0.25	0.17	0.17

Table S9. EDS element analysis of 100 wt% PSpF doped PDPIN film in different spots.

	Spot 1	**Spot 3**	**Spot 4**	**Spot 6**	**Spot 7**
Element	**Atomic %**	**Atomic %**	**Atomic %**	**Atomic %**	**Atomic %**
C K	66.55	63.78	65.18	66.73	59.1
N K	4.48	5.04	4.18	3.44	5.32
O K	3.93	4.95	4.11	7.96	5.62
F K	0	0.01	0	1.21	0.12
Si K	24.61	25.79	26.2	7.62	26.05
S K	0.29	0.27	0.2	1.38	0.71
Cr K	0.14	0.16	0.13	0.34	0.22

Table S10. EDS element analysis of 5 mol% N-DMBI doped PDPIN film in different spots.

	Spot 1	**Spot 2**	**Spot 3**	**Spot 4**	**Spot 5**
Element	**Atomic %**	**Atomic %**	**Atomic %**	**Atomic %**	**Atomic %**
C K	43.62	43.69	43.48	38.51	36.73
N K	9.71	9.2	8.87	11.56	13.98
O K	11.91	11.73	11.09	13.63	22.75
Si K	34.32	34.96	36.13	34.97	25.94
S K	0.25	0.22	0.25	1.15	0.36
Cr K	0.19	0.2	0.18	0.19	0.24

Table S11. EDS element analysis of 50 mol% N-DMBI doped PDPIN film in different spots.

	Spot 1	**Spot 2**	**Spot 3**	**Spot 4**	**Spot 5**
Element	**Atomic %**	**Atomic %**	**Atomic %**	**Atomic %**	**Atomic %**
C K	59.99	59.63	53.53	55.28	59.27
N K	5.74	6.15	5.74	7.64	5.91
O K	5.34	5.32	5.6	6.33	5.61
Si K	28.35	28.34	34.66	5.8	28.67
S K	0.43	0.4	0.31	0.59	0.38
Cr K	0.15	0.15	0.17	0.25	0.17

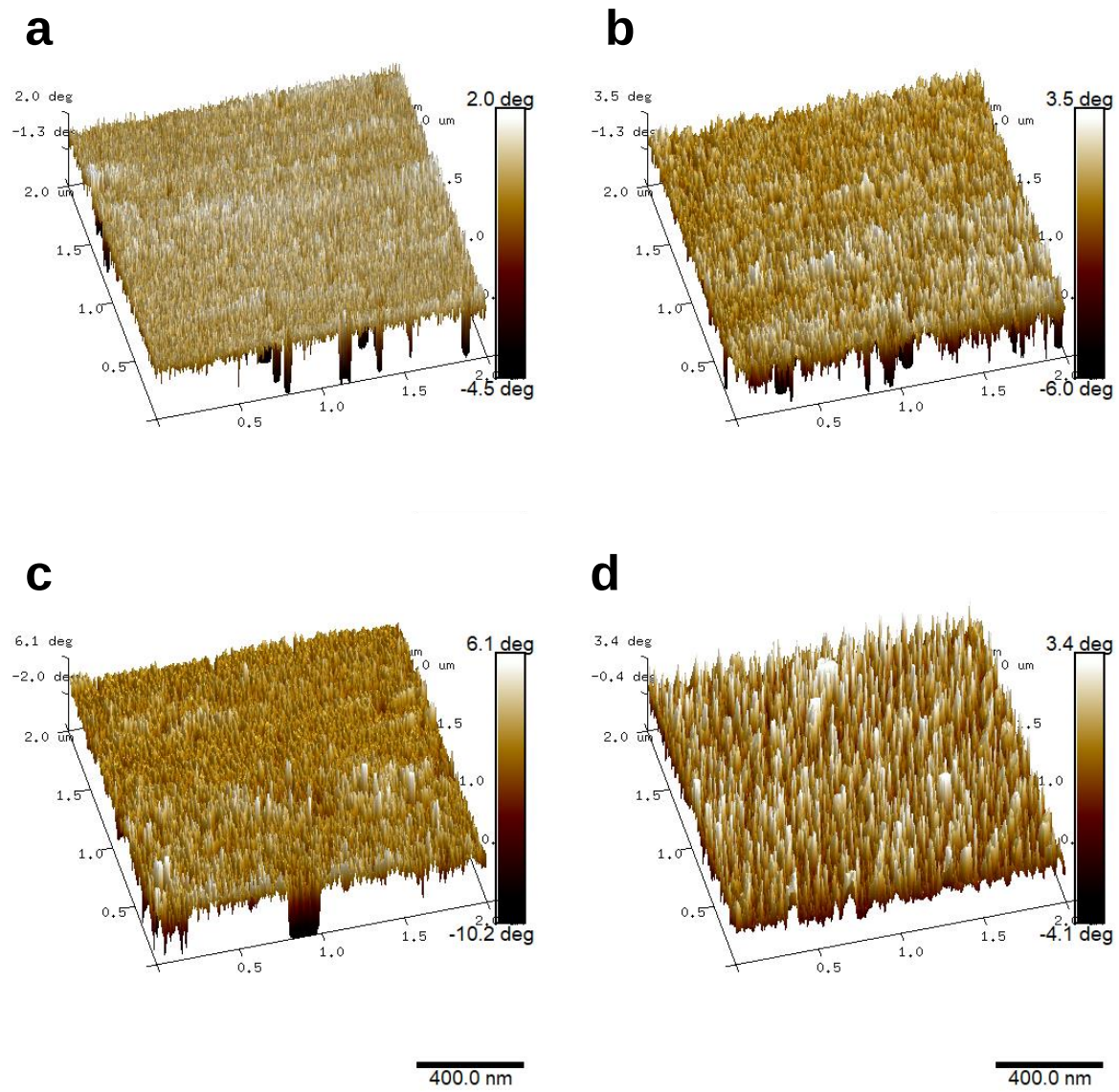

Figure S27. AFM phase images of a) pristine and b) 5, c) 30 and d) 75 mol% N-DMBI doped PDPIN films. The films were prepared with spin-coating method.

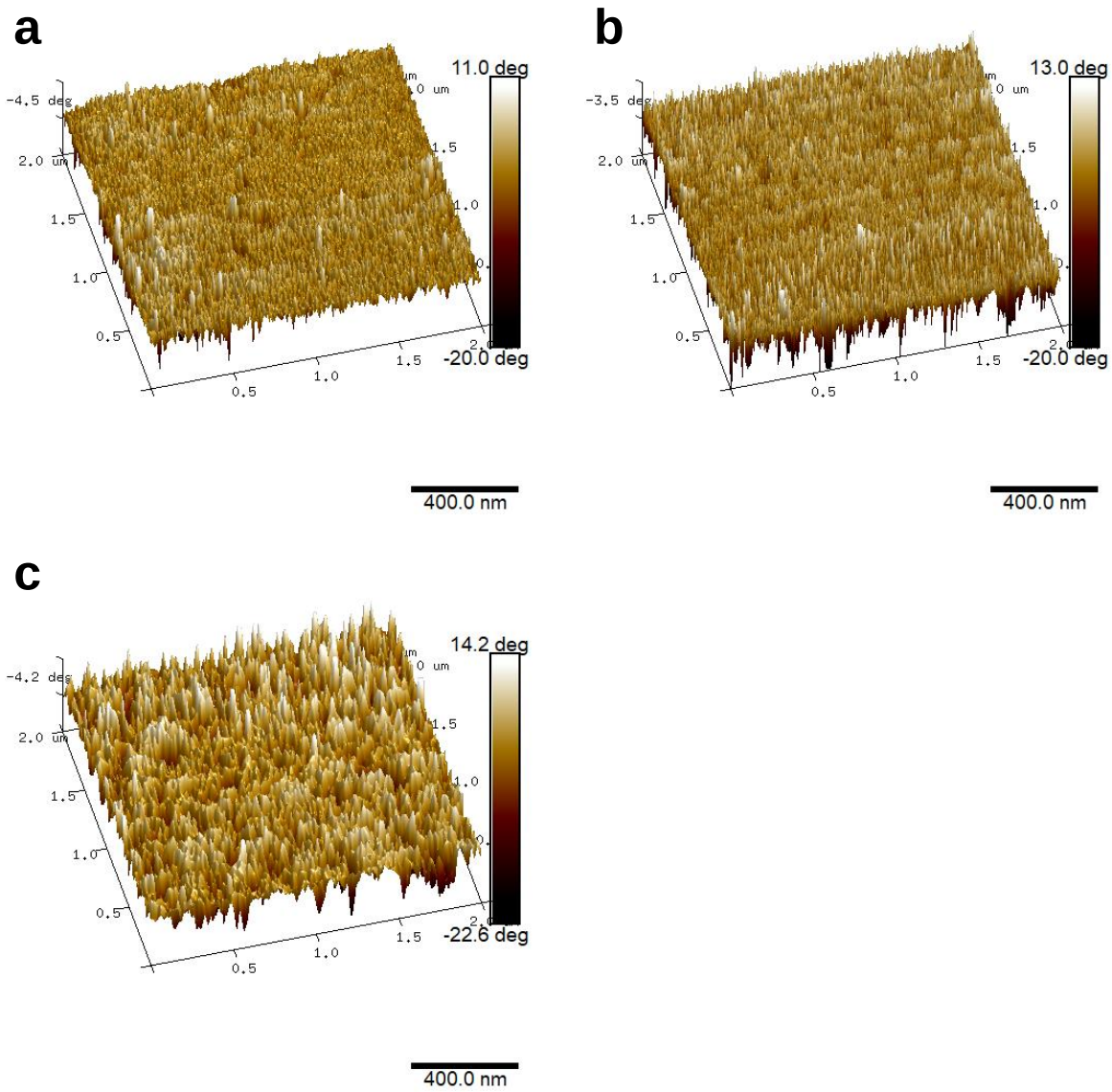

Figure S28. AFM phase images of a) 5, b) 50 and c) 100 wt% PSpF doped PDPIN films. The films were prepared with spin-coating method.

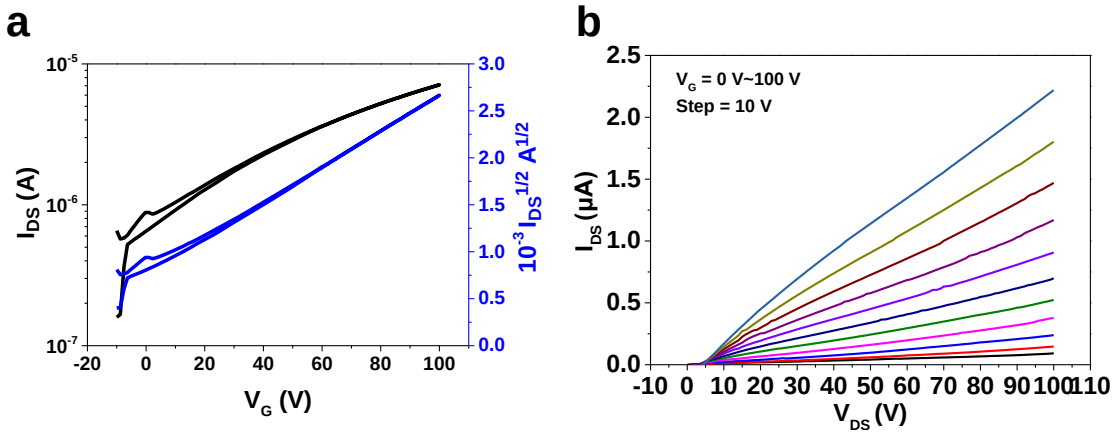

Figure S29. a) Transfer curves and b) out-put curves of prinstine PDPIN-based OFETs.

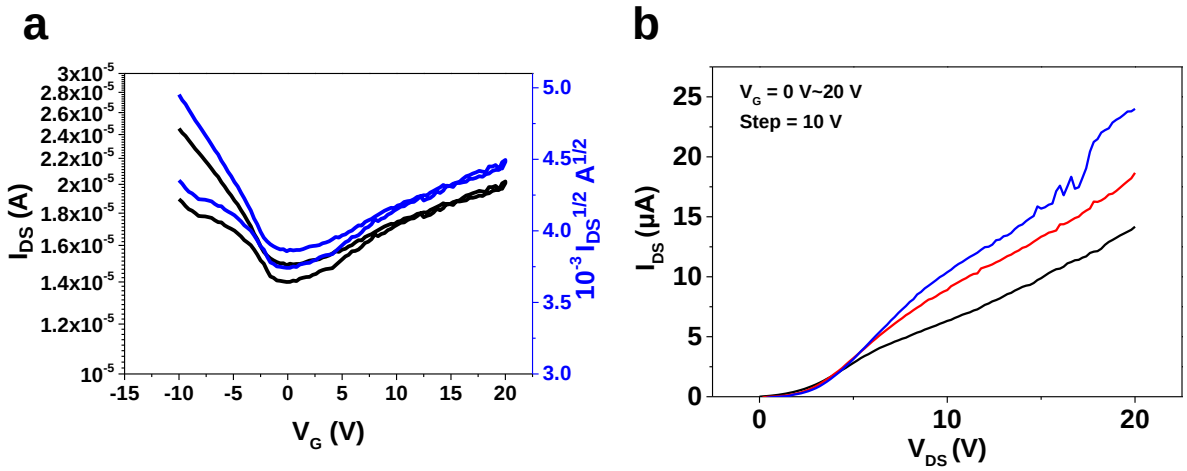

Figure S30. a) Transfer curves and b) out-put curves of 0.2 mol% N-DMBI doped PDPIN-based OFETs.

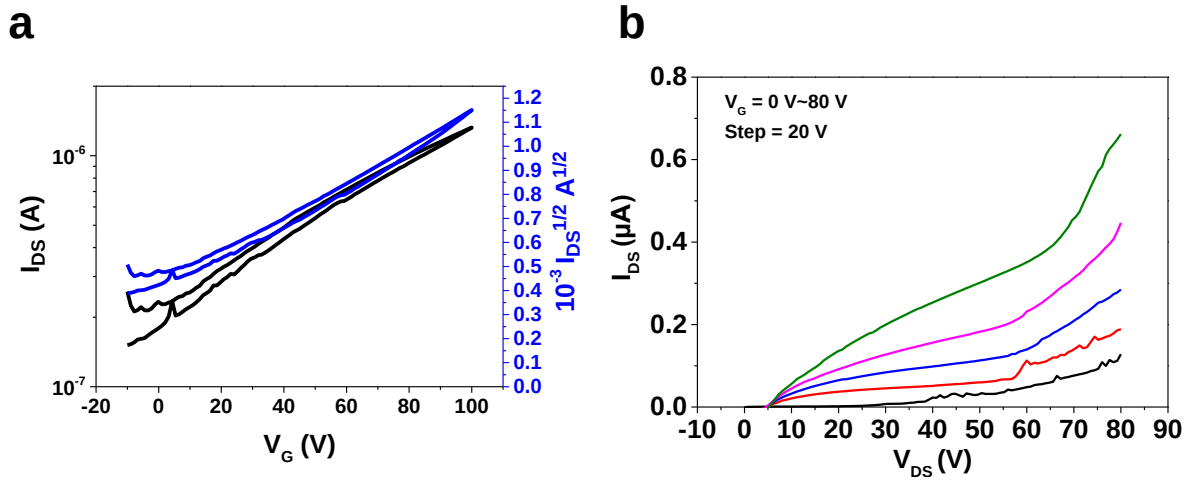

Figure S31. a) Transfer curves and b) out-put curves of 2 mol% N-DMBI doped PDPIN-based OFETs.

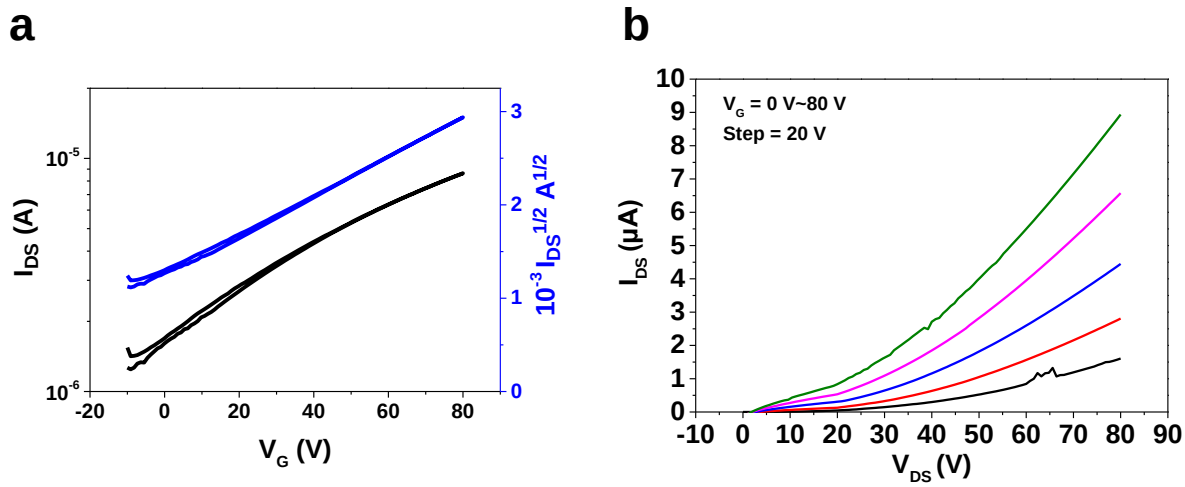

Figure S32. a) Transfer curves and b) output curves of 0.5 wt% PSpF doped PDPIN OFETs.

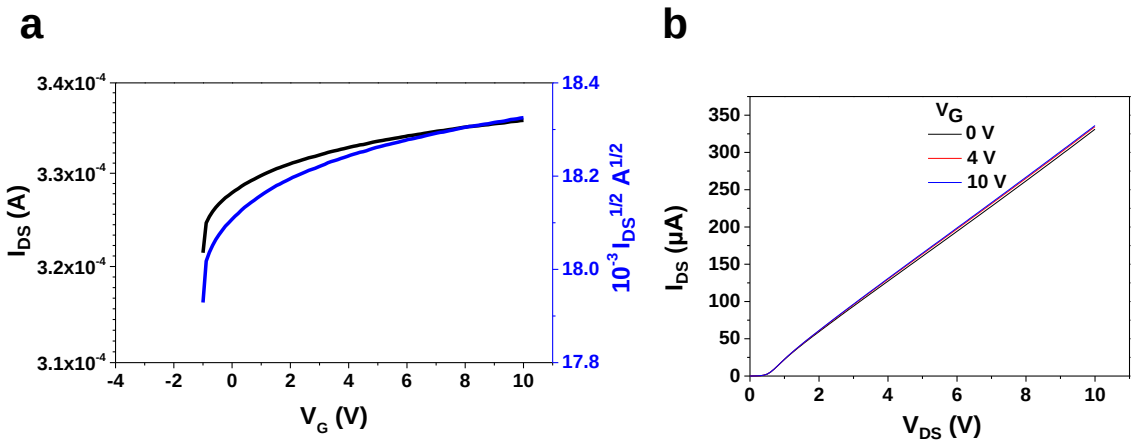

Figure S33. a) Transfer curves and b) output curves of 5 wt% PSpF doped PDPIN OFETs.

References:

[1] T. Lee, S. S. Panda, J. D. Tovar, H. E. Katz, *ACS Nano* **2020**, *14*, 1846-1855.

[2] J. Han, H. Fan, Q. Zhang, Q. Hu, T. P. Russell, H. E. Katz, *Adv. Funct. Mater.* **2021**, *31*, 2005901.

[3] a) D. G. Cahill, *Review of Scientific Instruments* **2004**, *75*, 5119-5122; b) J. L. Braun, S. W. King, A. Giri, J. T. Gaskins, M. Sato, T. Fujiseki, H. Fujiwara, P. E. Hopkins, *Applied Physics Letters* **2016**, *109*, 191905.

[4] a) X. Zhao, D. Madan, Y. Cheng, J. Zhou, H. Li, S. M. Thon, A. E. Bragg, M. E. DeCoster, P. E. Hopkins, H. E. Katz, *Adv. Mater.* **2017**, *29*, 1606921; b) H. Li, M. E. DeCoster, R. M. Ireland, J. Song, P. E. Hopkins, H. E. Katz, *Journal of the American Chemical Society* **2017**, *139*, 11149-11157.

[5] A. J. Schmidt, *Annual Review of Heat Transfer* **2013**, *16*.

[6] Z. Ge, D. G. Cahill, P. V. Braun, *Physical Review Letters* **2006**, *96*, 186101.

[7] A. Schmidt, M. Chiesa, X. Chen, G. Chen, *Review of Scientific Instruments* **2008**, *79*, 064902.

[8] R. M. Costescu, M. A. Wall, D. G. Cahill, *PhRvB* **2003**, *67*, 054302.

[9] P. E. Hopkins, J. R. Serrano, L. M. Phinney, S. P. Kearney, T. W. Grasser, C. T. Harris, *J. Heat Transfer* **2010**, *132*.

[10] C. Thomsen, H. T. Grahn, H. J. Maris, J. Tauc, *PhRvB* **1986**, *34*, 4129.

[11] X. Feng, X. Wang, *Thin Solid Films* **2011**, *519*, 5700-5705.
[12] a) O. Bubnova, Z. U. Khan, A. Malti, S. Braun, M. Fahlman, M. Berggren, X. Crispin, *Nature materials* **2011**, *10*, 429-433; b) D. G. Cahill, S. K. Watson, R. O. Pohl, *PhRvB* **1992**, *46*, 6131; c) D. G. Cahill, R. O. Pohl, *PhRvB* **1987**, *35*, 4067; d) J. A. Malen, K. Baheti, T. Tong, Y. Zhao, J. A. Hudgings, A. Majumdar, *J. Heat Transfer* **2011**, *133*; e) M. D. Losego, L. Moh, K. A. Arpin, D. G. Cahill, P. V. Braun, *Applied Physics Letters* **2010**, *97*, 011908; f) S. Shenogin, A. Bodapati, P. Keblinski, A. J. H. McGaughey, *Journal of Applied Physics* **2009**, *105*, 034906; g) H. Li, M. E. DeCoster, R. M. Ireland, J. Song, P. E. Hopkins, H. E. Katz, *Journal of the American Chemical Society* **2017**, *139*, 11149-11157.
[13] a) J. Han, C. Ganley, Q. Hu, X. Zhao, P. Clancy, T. P. Russell, H. E. Katz, *Adv. Funct. Mater.* **2021**, *31*, 2010567; b) T. Mukhopadhyaya, T. Lee, C. Ganley, P. Clancy, H. E. Katz, *ACS Applied Polymer Materials* **2022**, *4*, 2065-2080.
[14] G. Knizia, *J. Chem. Theory Comput.* **2013**, *9*, 4834-4843.
[15] B. Russ, A. Glaudell, J. J. Urban, M. L. Chabinyc, R. A. Segalman, *Nat. Rev. Mater.* **2016**, *1*, 16050.